46320 Loads, Aerodynamics & Control of Wind Turbines

Final Report:

Aeroelastic analysis and design of the Turkispain wind turbine

Authors:
Kaya Onur Dag, s111058
Emre Barlas, s110988
Alfonso Pérez-Andújar, s111672

Department of Wind Energy
Technical University of Denmark (DTU)
December 2012

Contents

List of Figures

List of Tables

Chapter 1

Introduction

This present report deals with the initial design stage of a 5 MW onshore wind turbine. This is an interdisciplinary iterative process during which fundamental knowledge from various fields is required. It is well known that in order to make wind energy competitive the cost energy has to be decreased. In that respect, current wind turbines are getting larger and larger. The reason for which a 5 MW turbine is chosen is the fact that there are some other existing options to compare to. The main goal is to model a turbine which represents an improved version of the existing ones.

Throughout the report, firstly the aerodynamical design was carried out. Secondly, the structural design was implemented, taking the final aerodynamic design outputs into account. Since Turkispain is a pitch regulated turbine, a controller had to be implemented. The input files were checked step by step with dummy turbines and finally the aeroservoelastic model was simulated. Ultimately, the annual energy production was calculated and and abbreivated version of required IEC design load cases was simulated. All this was done with the softwares HAWC2 and HAWCStab2 and Matlab. The specifications of the Turkispain wind turbine is listed in the table 1.

The contribution of the three group members was equal during the semester. In other words, all the members did all the parts.

Rated Capacity	5 [MW]
Rated Wind Speed	12 $[m/s]$
IEC Class	2B
Rotor Diameter	126 $[m]$
Cut In/Out Wind Speed	4 - 26 $[m/s]$
Swept Area	12668 $[m^2]$

Chapter 2

Aerodynamic Rotor Design

Aerodynamic rotor design is a compromise process between the aerodynamic efficiency of the blade and the structural demands of the entire wind turbine; it is the goal of the aerodynamicist to foresee these structural requirements and revise the aerodynamic design parameters (the very choice of the airfoils, for example, especially towards the root of the blade) so that also structural inputs are taken into account. This section is a step-by-step follow-up of [Aerodynamic Design of Wind Turbine Rotors, Christian Bak, September 2011], where indeed it is recommended to bear in mind the aforementioned advice regarding structural input.

2.1 One-point blade design

The one-point design process carried out in this section does not focus only on maximising the power, but also on other aspects, in an attempt to reduce the total cost of energy. These constraints affect both the design starting point and the output of the one-point design code. As an example, prior to anything came the choice of number of blades, 3 in this case (due to structural and esthetic considerations, among others), whilst one of the changes made to the blade at the very end was the airfoil characteristics at the root, as will be explained in detail further on.

Since one goal of this work is to challenge the NREL wind turbine rotor design, a number of aspects were directly chosen to match this wind turbine, for comparison purposes. Regarding just rotor design, these aspects are:

- *The number of blades:* Chosen to be 3, as in NREL. Furthermore, flickering of 2-bladed rotors is more annoying and, structurally, the bigger the number of blades, the smaller the chord and thus the smaller the thickness (if relative thickness is to be kept the same), which leads to structural problems.
- *The control type:* Pitch-regulated variable speed (PRVS), as in NREL. Furthermore, this saves fatigue to the whole turbine, versus stall-regulation, thereby lengthening the turbine lifetime and decreasing the cost of energy.

Considering that airfoil characteristics is perhaps the most important factor regarding aerodynamic efficiency, a careful choice of the airfoils was carried out, according to the following scheme:

- *Relative thicknesses*: Chosen to be 15%, 21%, 24% and 30%. 15% is the minimum chosen relative thickness due to the aforementioned structural considerations: on one hand, wind flow goes around slender blades more easily, meaning that the blades should be thin relative to their width; on the other hand, low relative thickness means that structurally, the blade will suffer. Lower t/c could have been placed tipwards, using stronger and more expensive materials to account for the extra slenderness, but then again the cost per blade must also be taken into account. On the other end of the t/c spectrum, the choice is 30%: even though a thicker airfoil was found in Nordtank's HAWC2 *.pc* file (namely the FFA-W36 airfoil), it was considered sufficient to obtain relative thicknesses over 30% (rootwards) by simply interpolating airfoils between $t/c = 30\%$ and $t/c = 100\%$ (at the root).
- *Airfoil type*:For each chosen relative thickness, the aerodynamic properties of different airfoils are depicted in figures 2.1 to 2.4. These plots depict experimental data of clean airfoils, since no data for LER was found for

any of the airfoils. Note that (*i*) these data correspond to 2D calculations, so a future 3D correction had to be implemented, (*ii*) the range of angle of attack for these experimental data is by all means not wide enough for HAWC2 (it needs angles of attack of each airfoil to span from $-180°$ to $180°$). Thus, as will be explained later, after applying the 3D correction to the experimental data, these were merged with data from the sample *.pc* files found in HAWC2 in order to account for bigger and smaller angles of attack.

The characteristics that were taken into account when choosing one airfoil among the many, for each relative thickness, were the following:

- *High lift-drag ratio in wide range of C_l values (i.e. in a wide range of angle of attack).*
- *Regular lift curve.* A linear behaviour for small angles of attack is wanted. Even though the behaviour of the airfoils lift coefficient after stall is irrelevant, since Turkispain has been designed to be pitch-controlled, a choice of C_l vs α curves with smooth . After all, pitching towards feathering decreases the angle of attack in order to reduce torque. It should be mentioned that the choice of a pitch control was made in order to be able to compare the results to NREL, as well as in an attempt to render a better aerodynamic design by alleviating loads at high angles of attack.

These considerations were applied to all the airfoils displayed in figures 2.1 to 2.4, for all selected thicknesses. The offset values seen for relative thickness 15% and 21% are experimental offset values.

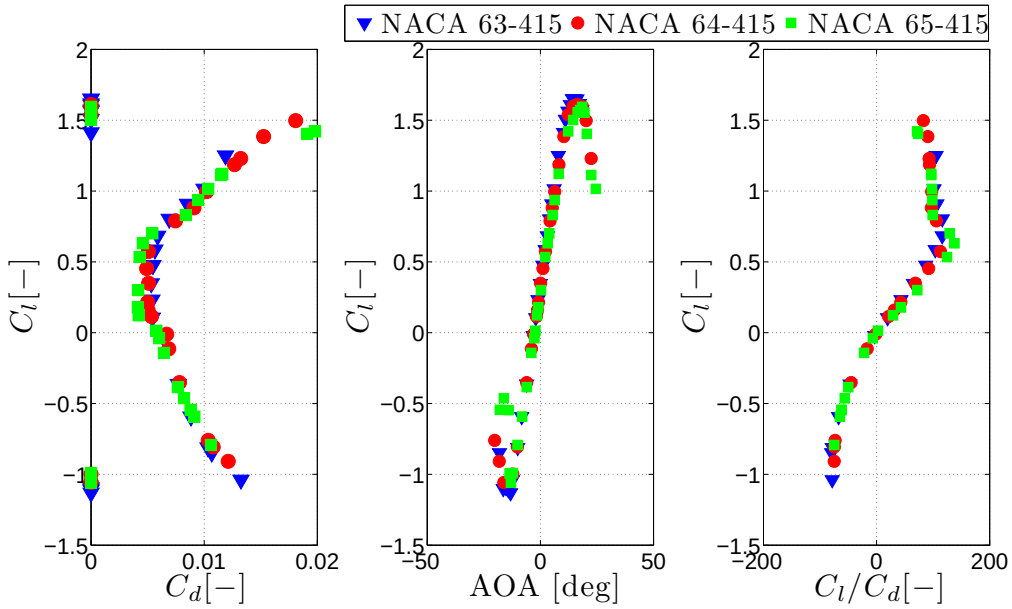

Figure 2.1: $t/c = 15\%, Re = 6 \cdot 10^6$

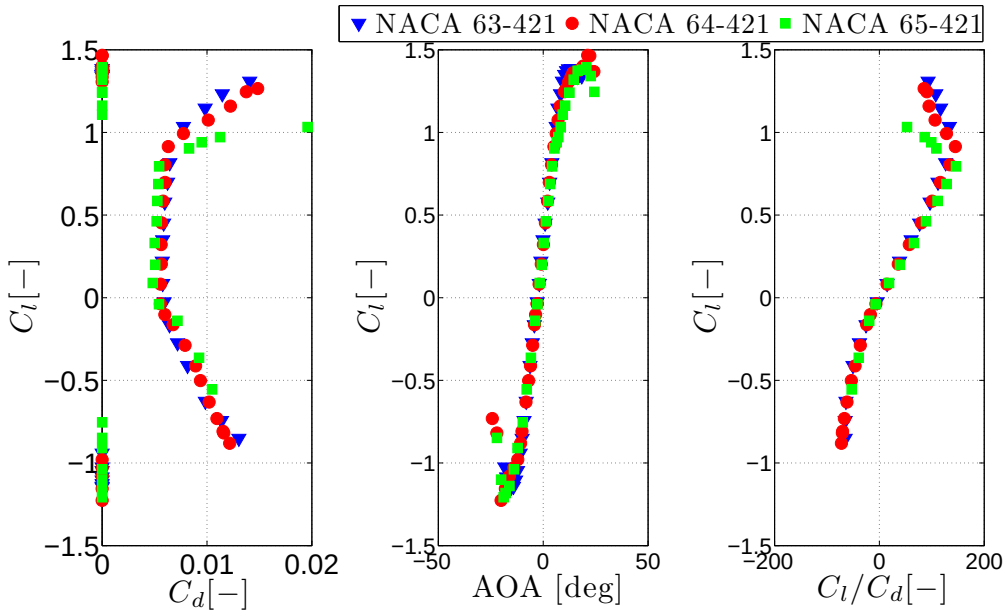

Figure 2.2: $t/c = 21\%, Re = 6 \cdot 10^6$

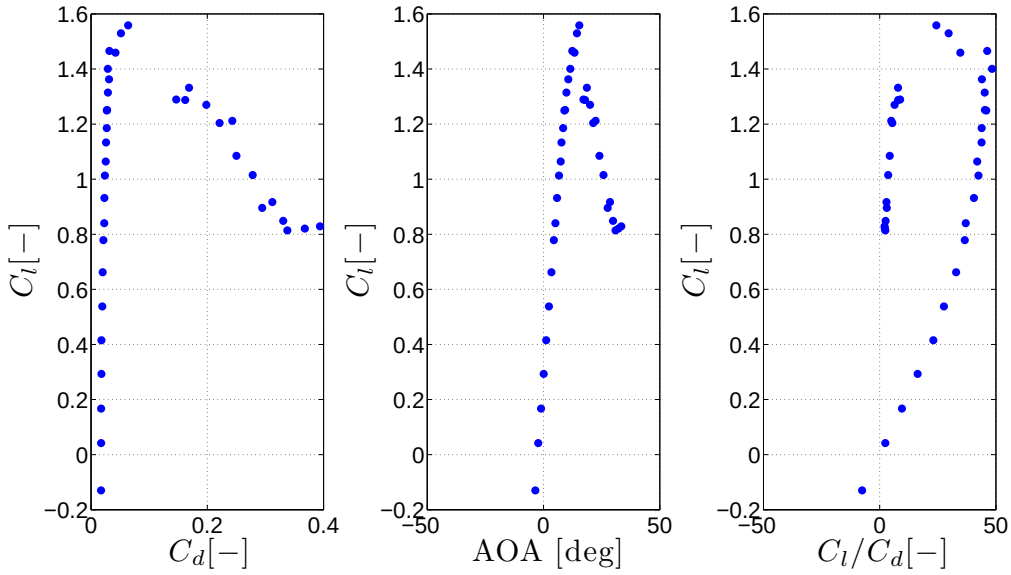

Figure 2.3: $t/c = 24\%, Re = 1.47 \cdot 10^6$

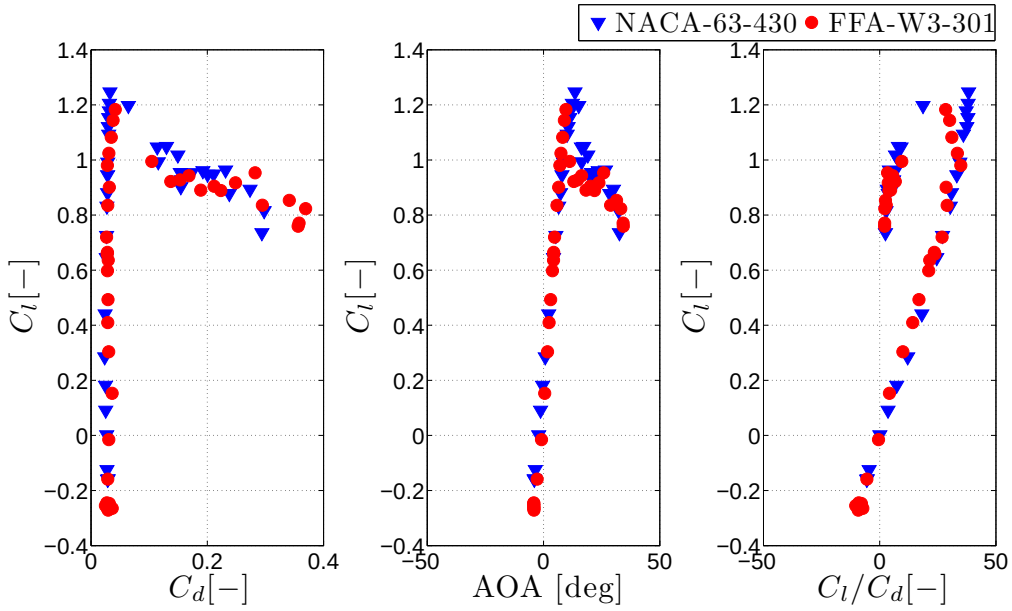

Figure 2.4: $t/c = 30\%, Re = 1.45 \cdot 10^6$

The above pre-selection of airfoils was not wider (does not show all the available airfoils in the catalogue) for varying reasons:

- For $t/c = 15\%$ and 21%, only NACA airfoils 63-415, 64-415 and 65-415 were pre-selected due to Reynolds number considerations: Re should lie somewhere between 75000 and 150000 times the rotor radius (rule of thumb), and thus for Turkispain's radius, $R = 61m$, $Re \in (4.6 \cdot 10^6, 9.2 \cdot 10^6)$. This means that the most suitable data for these thicknesses was the airfoil catalogue NACA WS $Re = 6 \cdot 10^6$.
- For $t/c = 24\%$, the competition was held just between two airfoils, FFA-W3-241 and Risoe-A1-24, because these were the only available. Even though the A1-24 has clearly a larger glide ratio for a wide range of C_l, as seen in figure 2.3, FFA is the final choice because no airfoil coordinates were found for A1-24.
- For $t/c = 30\%$, both airfoils NACA and FFA have $Re = 1.4 \cdot 10^6$. Even though this is way below the minimum recommended Re, again this was the only data available for this relative thickness.

From the above airfoils, only one was chosen for each relative thickness, as seen in figures 2.5 to 2.8.

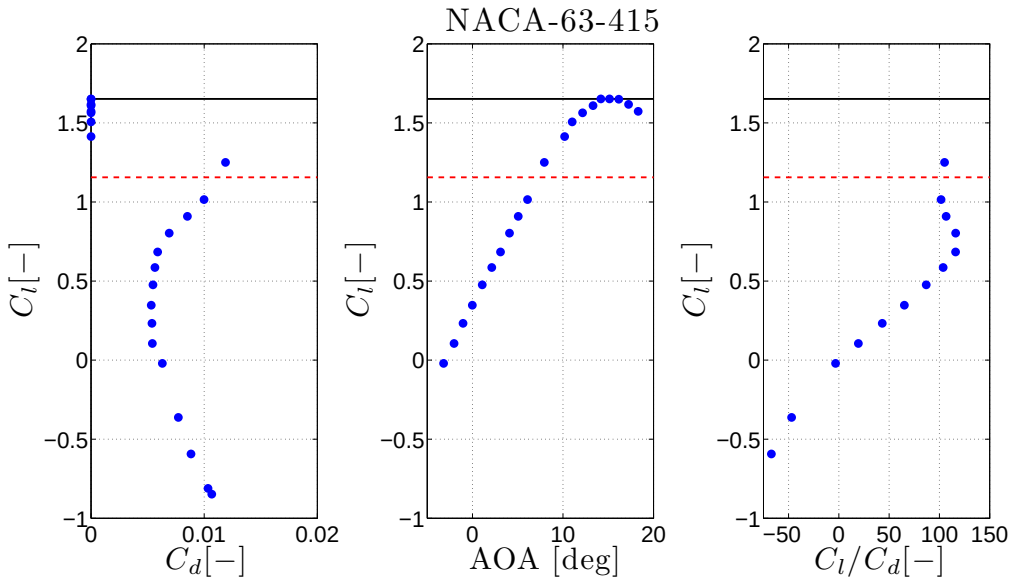

Figure 2.5: Chosen airfoil for $t/c = 15\%, Re = 6 \cdot 10^6$

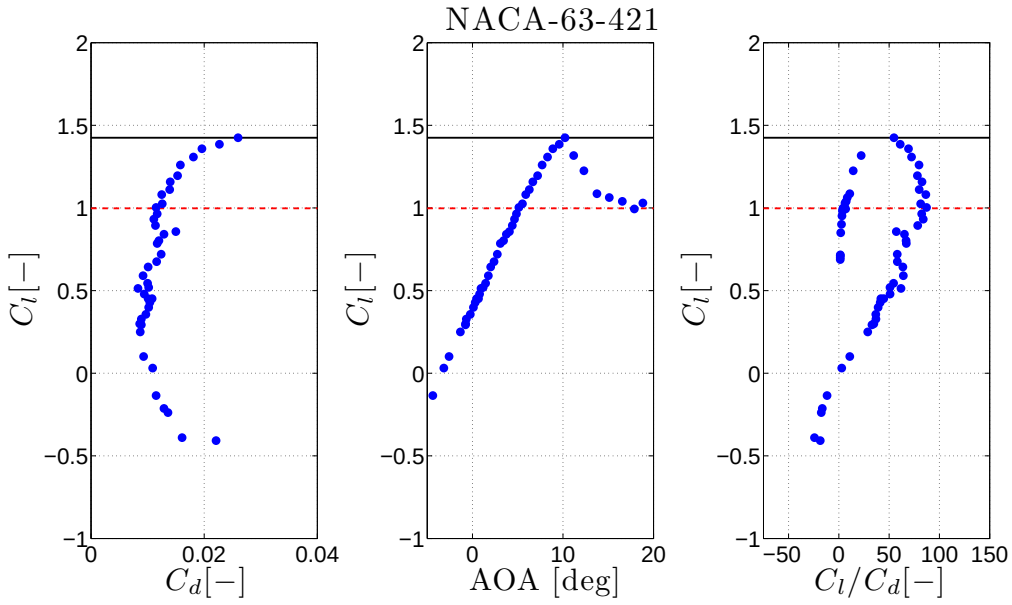

Figure 2.6: Chosen airfoil for $t/c = 21\%, Re = 6 \cdot 10^6$

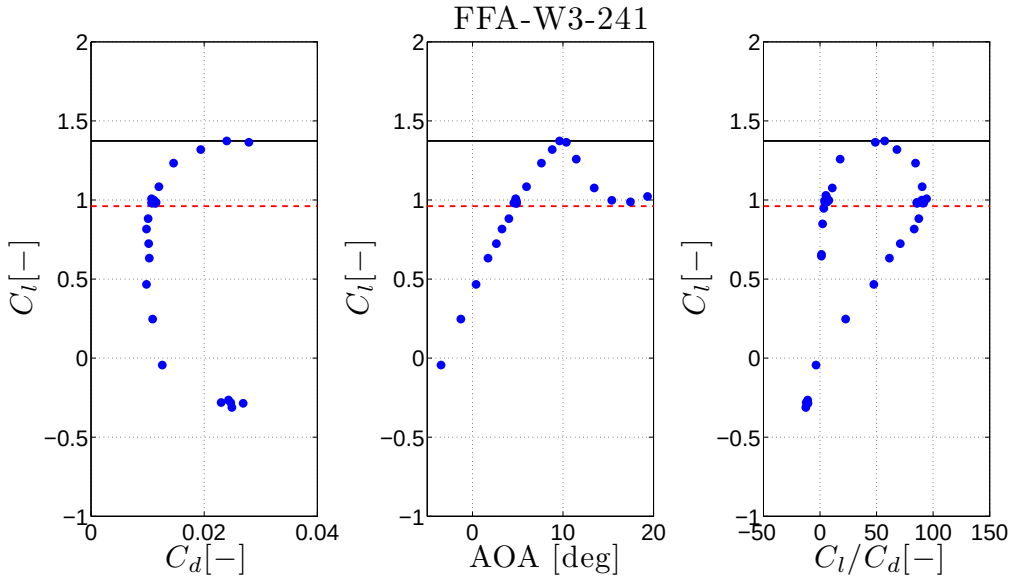

Figure 2.7: Chosen airfoil for $t/c = 24\%, Re = 1.47 \cdot 10^6$

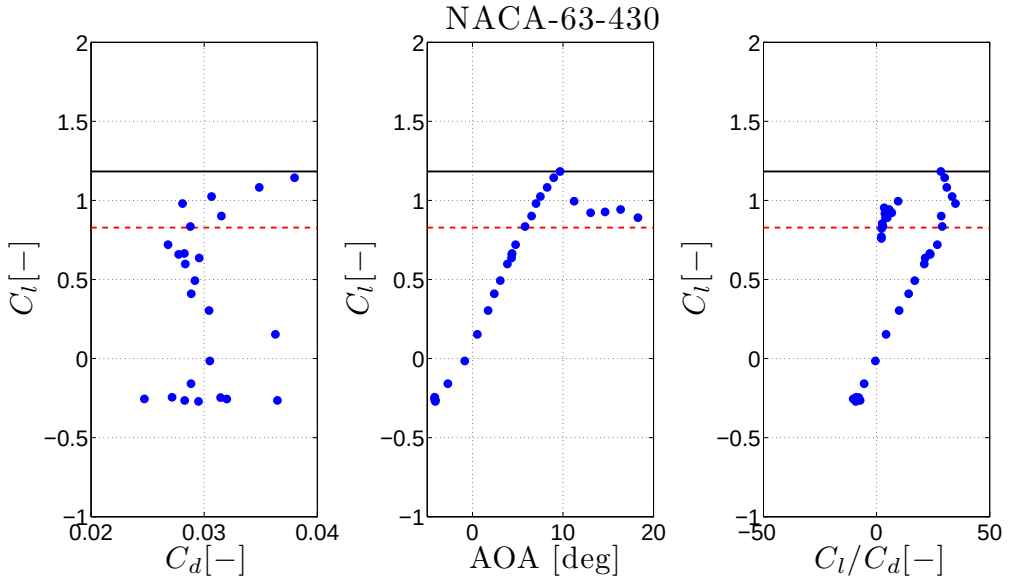

Figure 2.8: Chosen airfoil for $t/c = 30\%, Re = 1.45 \cdot 10^6$

As indicated in the figures above, the design C_l, C_l/C_d and α was chosen by following the procedure explained below.

- The maximum C_l was chosen (black line), and reduced 30% (dashed line) to account for:
  - Possible gusts that may take the blade into stall before the controller has time to react.
  - The fact that these data are for clean airfoils, i.e the airfoil characteristics displayed in the figures are an over-prediction of the operational aerodynamics. This is why 30% has been used, instead of 20%, as would have been done for LER data.
- Corresponding glide ratios and angles of attack were chosen, according to the dashed line.

The next step in the one-point design procedure was to construct three functions depending on the variable t/c. These are $C_l = C_l(\frac{t}{c})$, $\frac{C_l}{C_d} = \frac{C_l}{C_d}(\frac{t}{c})$ and $\alpha = \alpha(\frac{t}{c})$. For information on how to build these functions, refer to [Aerodynamic Design of Wind Turbine Rotors, Christian Bak, September 2011], but it should at least be noted that for the non-linear part, cubic interpolation was used. These functions are shown in the figures below.

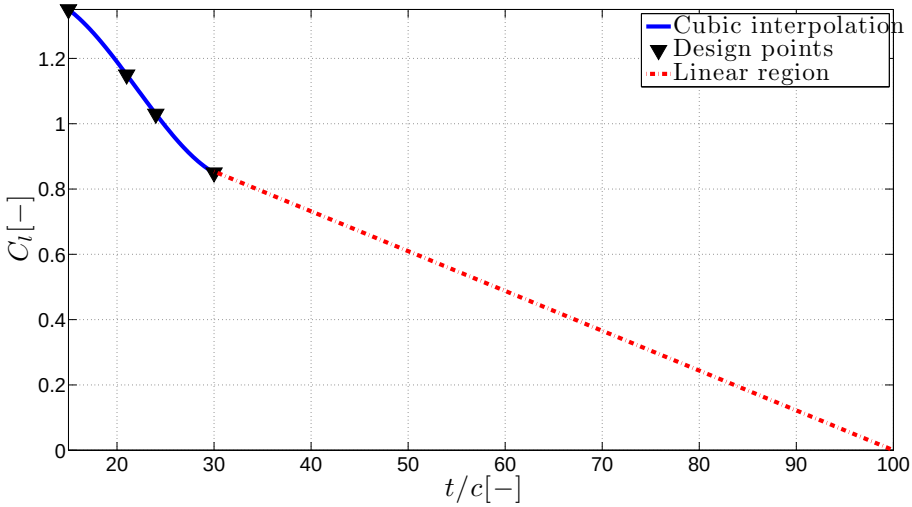

Figure 2.9: Design C_l.

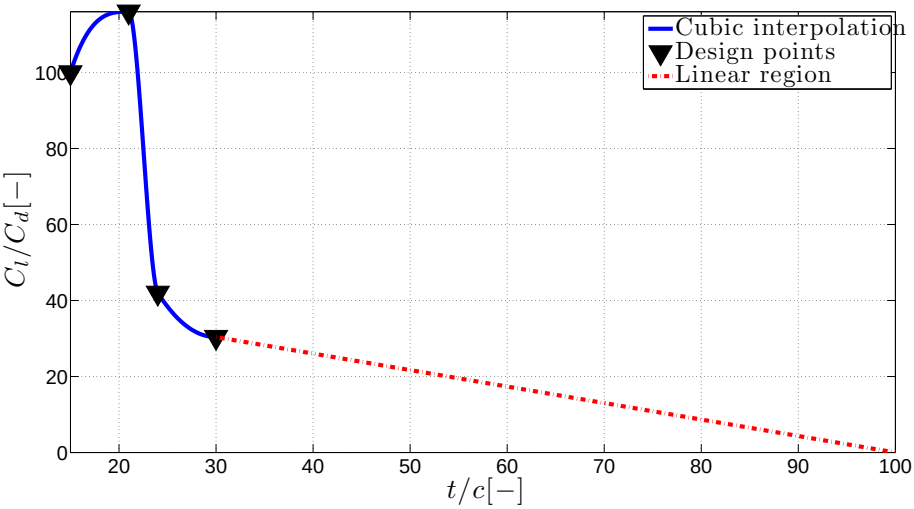

Figure 2.10: Design C_l/C_d.

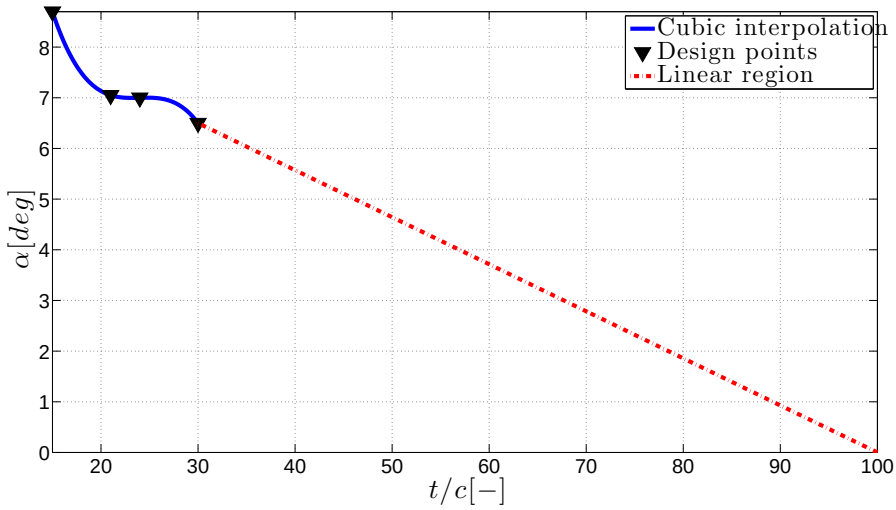

Figure 2.11: Design α.

It follows to run an iterative design code, where the goal is to optimise the chord distribution of the blade, in order to design an aerodynamically optimised rotor. The pre-conditions were:

- *An optimal axial induction factor,* $a = 1/3$.
- *A certain input thickness.* This was taken from NREL in the first place but was transformed to a more slender distribution because the first output relative thickness was not smooth. This smoothed version of NREL's thickness is shown in figure 2.12.
- *A certain radius vector.* The radial input started at first from $0m$ up to almost the tip (i.e. almost $63m$, due to computational errors arising at the tip). However, it was preferred to instead run the one-point design code from $5.1m$ on. The main reason for this is that the twist outputted by the code, for points very close to the root, was very big (around $70°$) due to the configuration of the velocity triangle in these sections. Thus, after running the code from $5.1m$ tipwards, a cylinder was added to account for the missing root part. The power production that would be gained by building a twisted structure all the way from tip down to root would not pay off the extra cost of building a blade with such a twist (structurally it would be a feat). In fact, this drop in C_p in the blade with the added cylindrical root, with respect to the fully-twisted blade, is investigated further on and is found to be very small.
- *A chosen maximum chord.* It was set to $4m$ for economic and transport reasons.

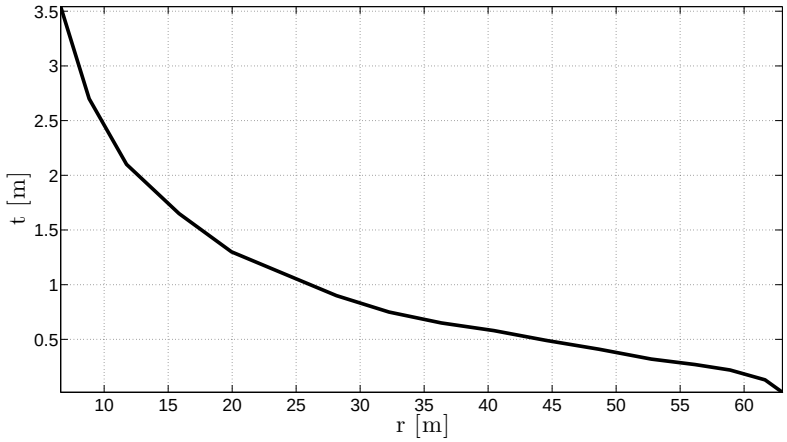

Figure 2.12: Smoothed input thickness.

With the smoothed input thickness shown in 2.12, the design code was finally run for a random choice of tip speed ratio $\lambda = 9$. The results are shown in figures 2.13 and 2.14, before and after adding the cylindrical root.

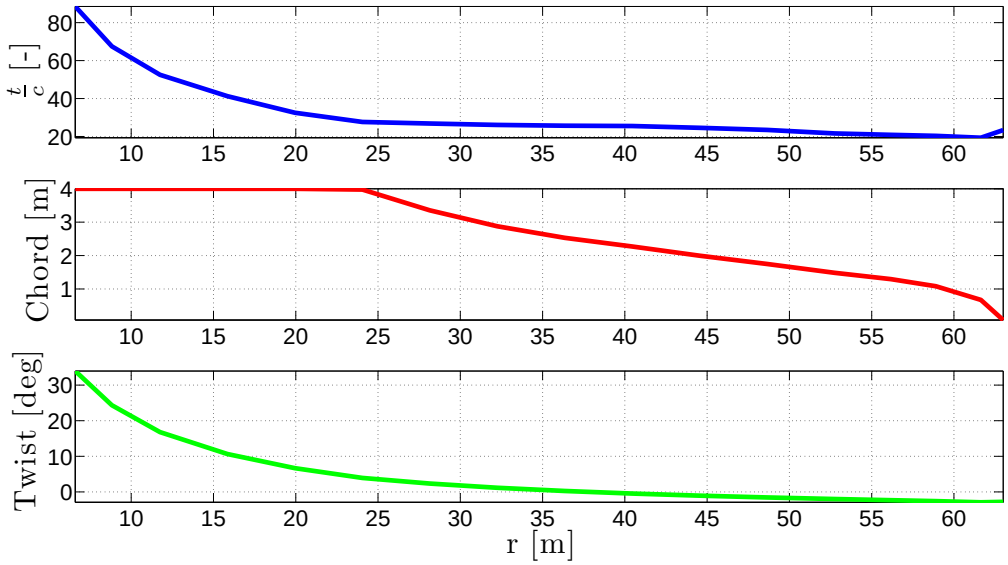

Figure 2.13: Blade design without root.

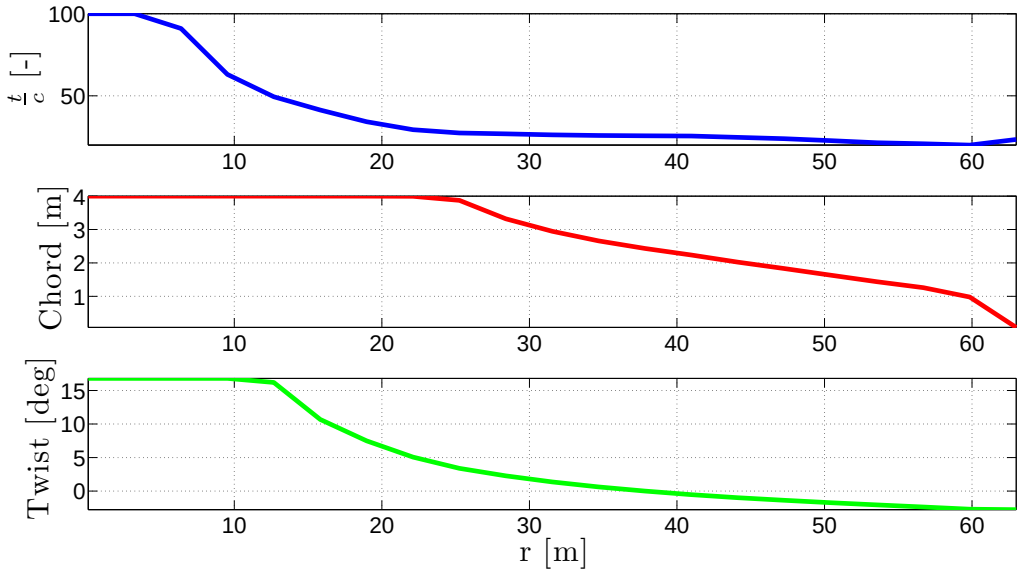

Figure 2.14: Blade design with root.

There are three main differences between 2.13 and 2.14:

- In the cylindrically-extended blade, 2.14, the tubular extension was done by assigning $t/c = 100\%$ to each blade section from $0m$ to $5.1m$.
- The twist of this added cylindrical root, as seen from 2.14, was set to the value of the twist at $r = 10m$, i.e. higher twist angles have been entirely discarded rootwards.
- The chord along this newly added section was set to maximum chord, and thus there is an updated thickness for Turkispain, given by the extended versions of chord and relative thickness, as $t_{extended} = c_{max}(\frac{t}{c})_{extended}$. This is shown in figure 2.15.

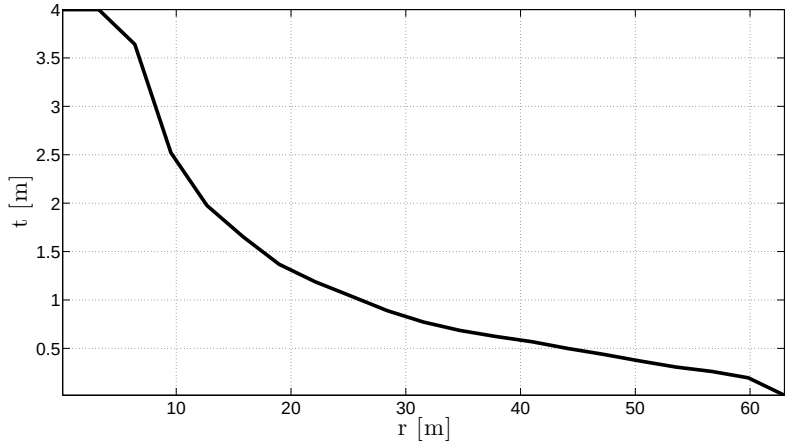

Figure 2.15: Updated input thickness, including root.

The three distributions seen in 2.14 are the main input for the blade 3D shape construction, as well as for an important part of its structural design. There is a major fact to highlight: the 15% relative thickness does not

appear at any radial section of the blade, meaning that the design code "preferred" the other airfoils in terms of energy optimisation ($a = 1/3$) because, as seen in figure 2.5, the glide ratio is not optimal at design C_l. This is so because, as explained, the procedure to follow was that design C_l should be 70% of maximum C_l. However, as a side note, the C_p obtained if the design C_l for $t/c = 15\%$ had been chosen at maximum glide ratio, will be investigated further on.

Local characteristics outputted by the one-point design code can be seen in figure 2.16.

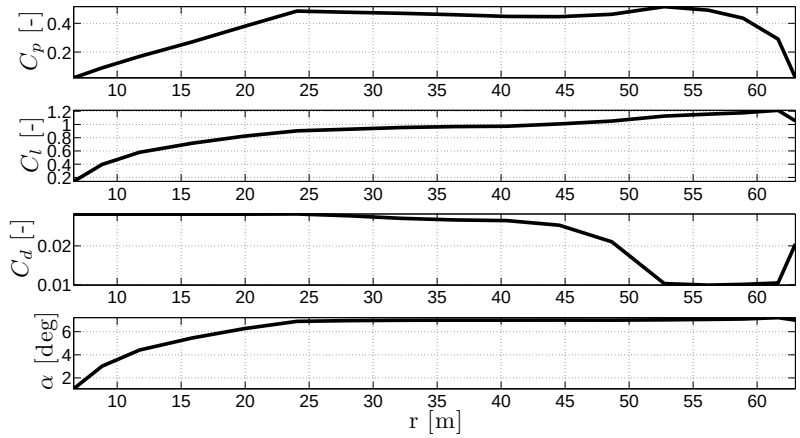

Figure 2.16: Local design characteristics of the blade.

2.2 3D correction of coefficients and BEM validation

A BEM code [41314 Wind Turbine Technology and Aerodynamics, DTU, 2011] was used to validate the blade design. In order to do this, the lift and drag coefficients of the 4 chosen airfoils were interpolated along the whole blade, as a function of the angle of attack, i.e. from $-180°$ to $180°$. A circular "airfoil" with $t/c = 100\%$ was included for the root part, with values of $C_l = 0$ and $C_d = 0.5$ for all angles of attack. These coefficients were corrected for 3D effects using HAWC 3D Profiler, which corrects only up to $\pm 45°$. This means that for $\alpha \notin [-45°,45°]$, the same uncorrected coefficients have been used, and a smoothing job with AF Tool had to be done at around $\pm 45°$ in order to smoothen the gap between corrected and uncorrected coefficients. This is shown in figures 2.17 to 2.24.

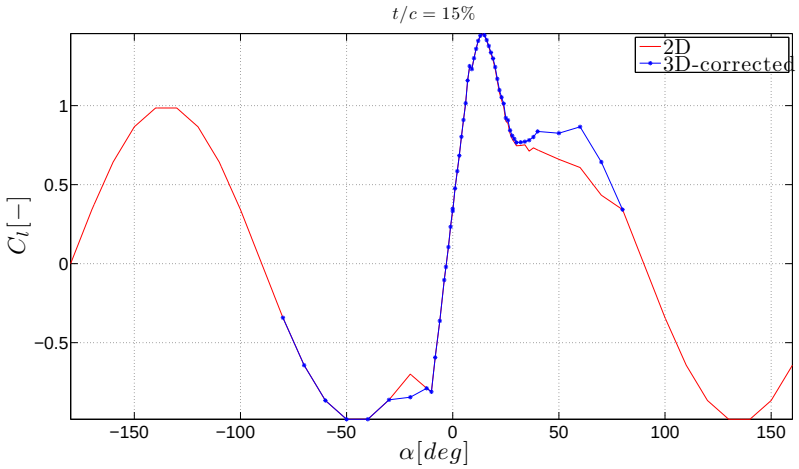

Figure 2.17: 3D-corrected C_l for NACA 63-415.

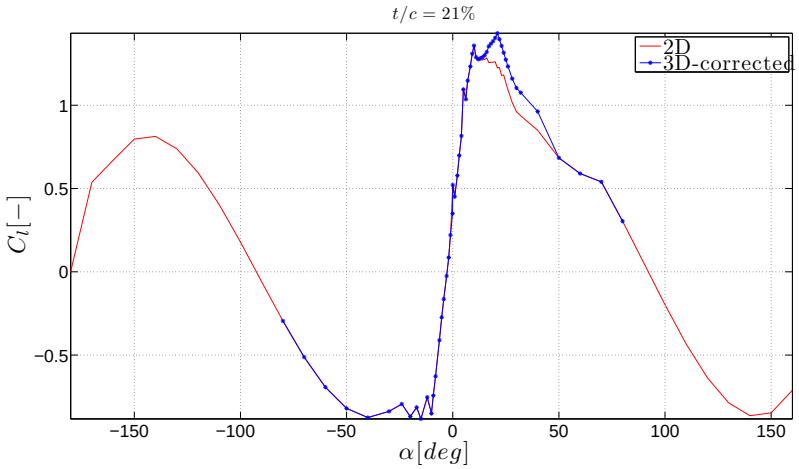

Figure 2.18: 3D-corrected C_l for NACA 63-421.

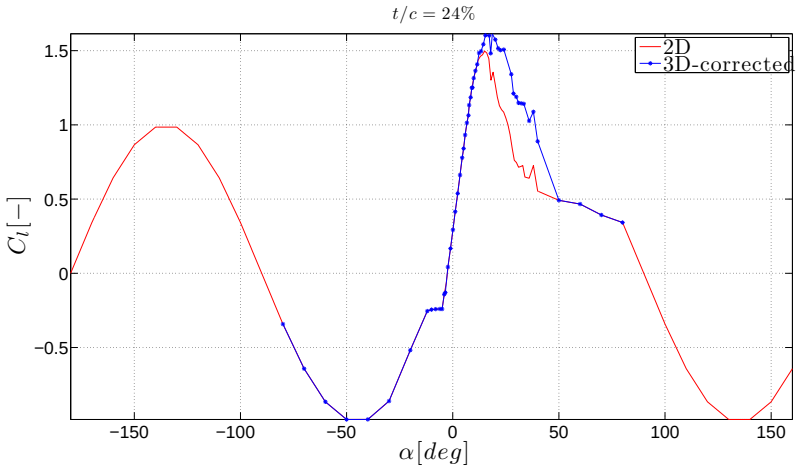

Figure 2.19: 3D-corrected C_l for FFA-W3-241.

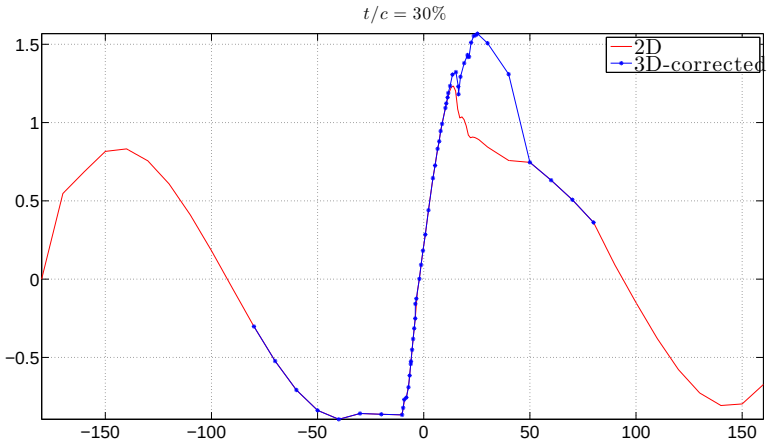

Figure 2.20: 3D-corrected C_l for NACA 63-430.

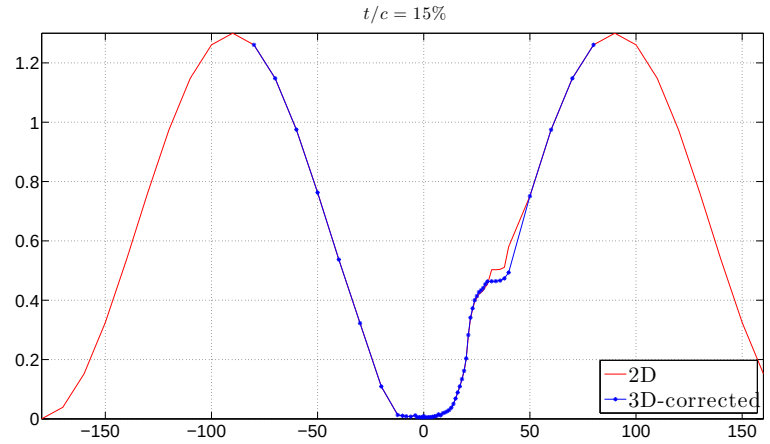

Figure 2.21: 3D-corrected C_d for NACA 63-415.

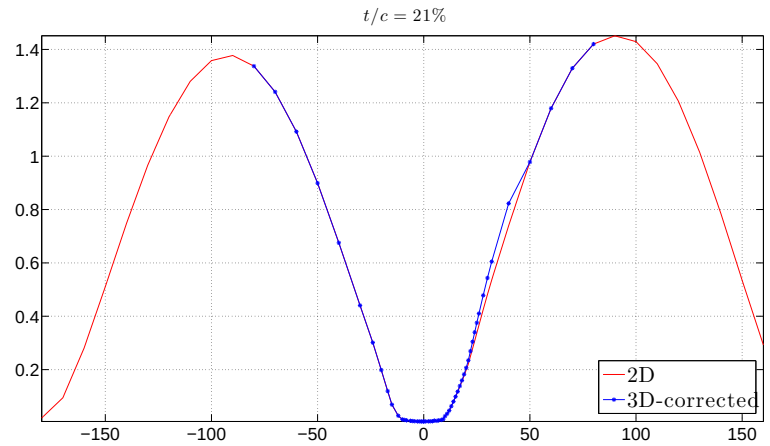

Figure 2.22: 3D-corrected C_d for NACA 63-421.

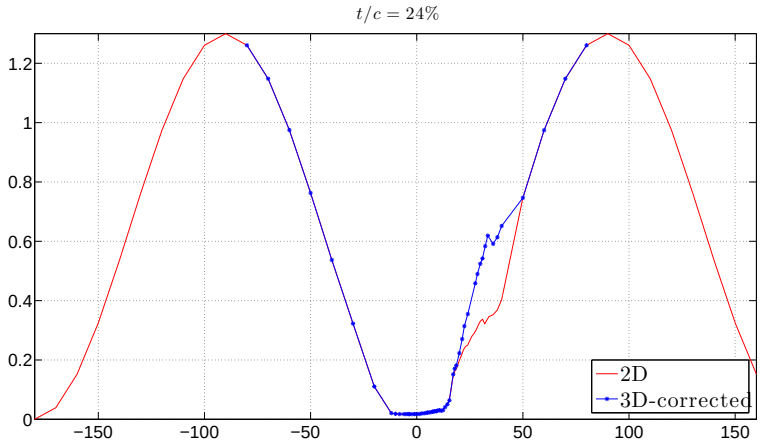

Figure 2.23: 3D-corrected C_d for FFA-W3-241.

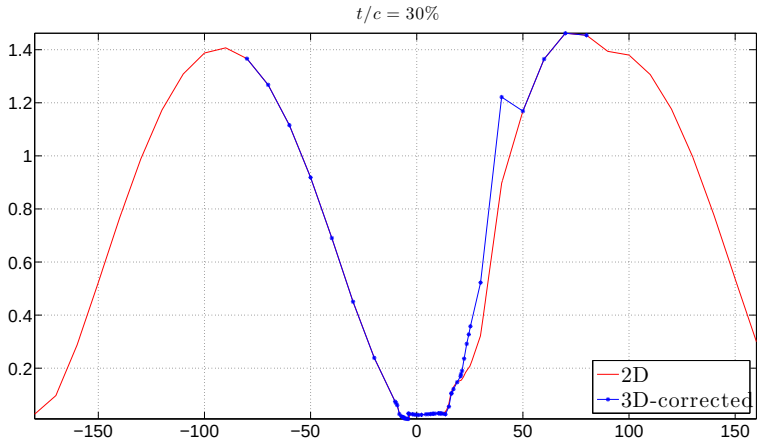

Figure 2.24: 3D-corrected C_d for NACA 63-430.

With these values, the first BEM calculation was Turkispain's rotor maximum C_p, as well the tip speed ratio and pitch angle at which this occurs. This is shown in figure 2.25.

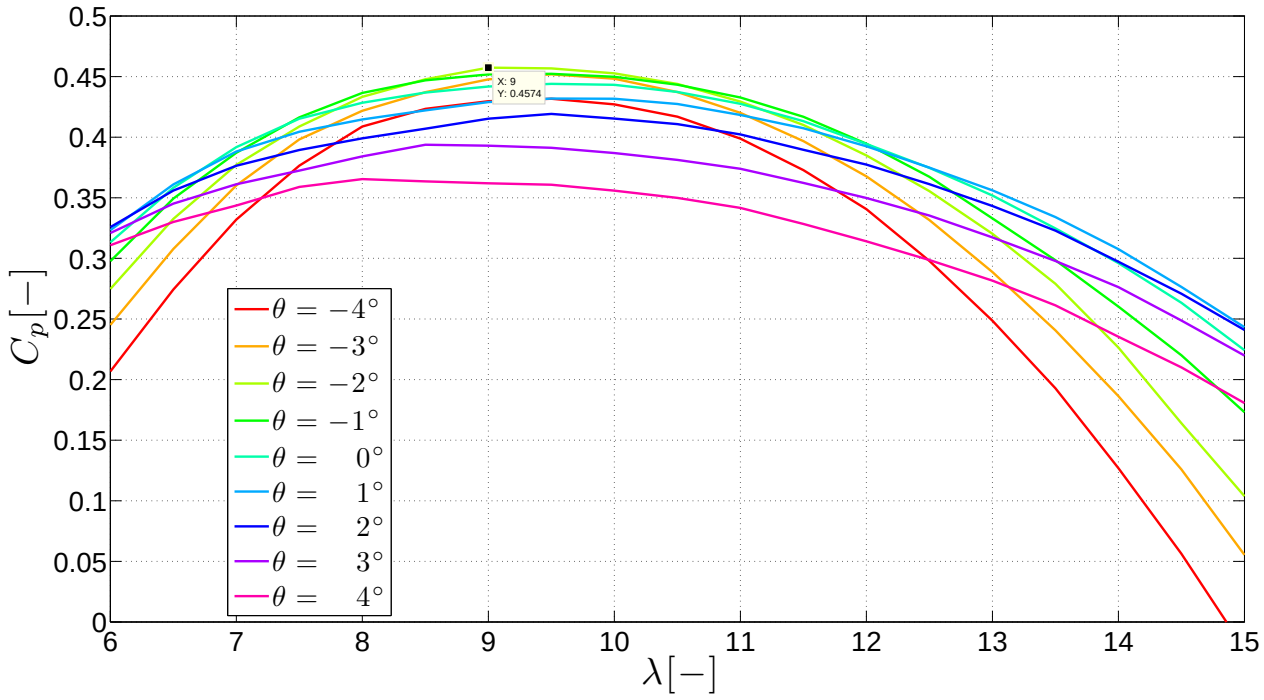

Figure 2.25: C_p vs λ, cylindrical, non-twisted root. $C_{p,max} = 0.4574$ found at λ_{opt}=9 and $\theta_{opt} = -2°$.

Figure 2.25 shows that the initial choice of $\lambda = 9$ was in fact λ_{opt}, giving the maximum power coefficient for a pitch angle of $-2°$. The fact that maximum C_p is obtained at design tip speed ratio means that the design lift of each airfoil was in fact the lift where maximum lift-drag ratio is found (this was not the case, as seen earlier, for $t/c = 15\%$, and this is why it is not present in the blade). Moreover, this ensures that the rotor will unlikely run into stall when a gust comes, and that it will not exceed noise regulations, since it operates where it has been designed to operate, as shown by the BEM code.

It is worthwhile investigating (as promised earlier) that a fully-twisted version of Turkispain's blade, down to the root, does in fact not add considerable C_p, as shown in 2.26.

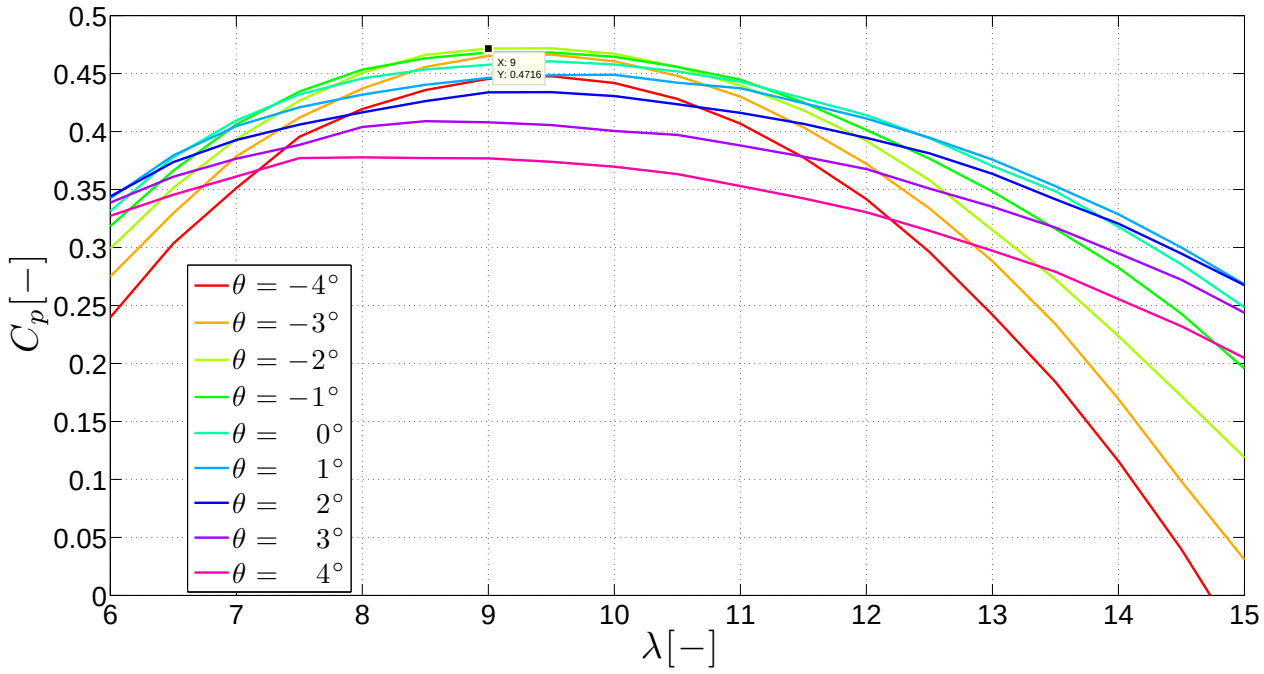

Figure 2.26: C_p vs λ, twisted root. $C_{p,max} = 0.4716$ found at λ_{opt}=9 and $\theta_{opt} = -2°$.

As was also promised earlier, the C_p of the blade that would have resulted if the design C_l had been changed only for $t/c = 15\%$, to coincide with maximum glide ratio, is shown below in 2.27.

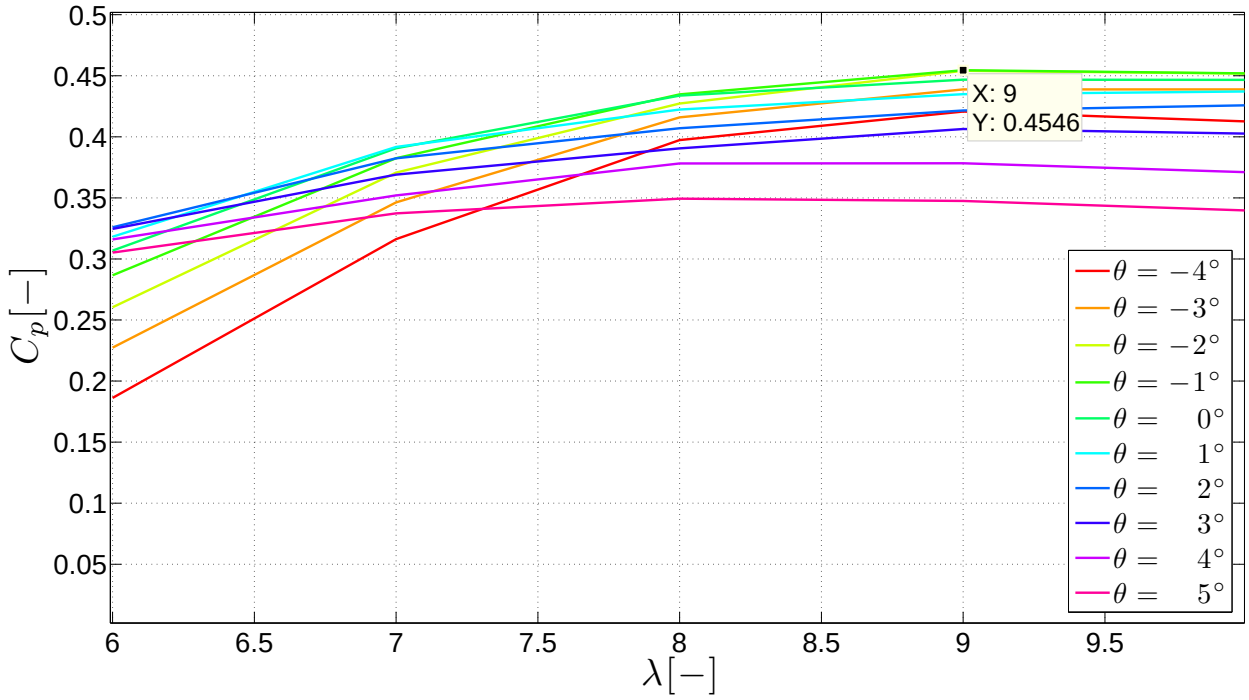

Figure 2.27: C_p vs λ, cylindrical, non-twisted root. Shift in glide ratio for $t/c = 15\%$. $C_{p,max} = 0.4546$ found at λ_{opt}=9 and $\theta_{opt} = -2°$.

The C_p is lower than for the twisted case, where the 15% remained unchanged. Thus, a twisted root means, in Turkispain's case, a higher energy yield than the one obtained when only optimising the glide ratio of the outermost airfoil.

However, for clarity purposes: the blade design is finally chosen to have no twist at the cylindrical root, i.e. a $C_{p,max} = 0.4574$ found at λ_{opt}=9 and $\theta_{opt} = -2°$, with the design parameters (lift and drag coefficients and angle of attack) depicted in figures 2.5 to 2.8. However, the initial pitch angle was changed from the optimum value of $-2°$ to $2.5°$, as seen in 2.28. This is explained further.

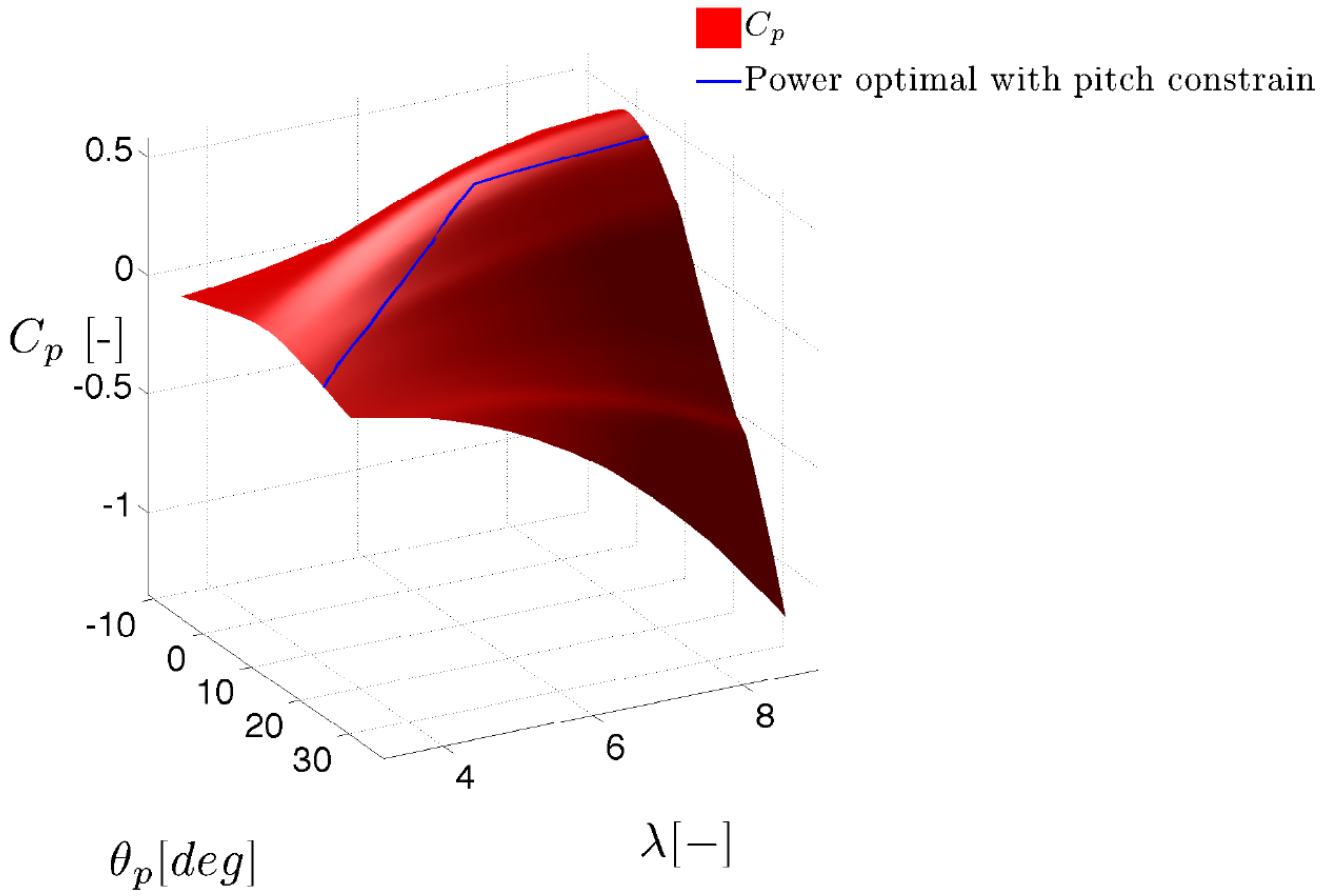

Figure 2.28: Surface C_p

Another good validation check is to ensure that when running the validation BEM at design $\lambda = 9$, the BEM-calculated C_l and C_d match the design C_l and C_d. This comparison is shown in figure 2.33, as a function of the radius.

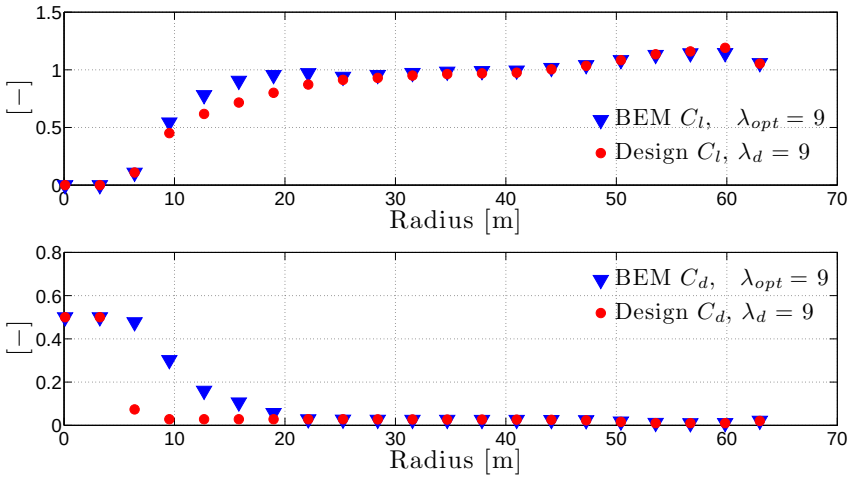

Figure 2.29: Design and BEM-calculated C_l and C_d.

The match is generally fair, except towards the root, where the BEM-calculated coefficients are shifted; this is however caused by the interpolation between the thickest chosen airfoil, $t/c = 30\%$, and $t/c = 100\%$ and thus, for airfoils with relative thicknesses higher than 30%, the BEM-calculated C_l and C_d are already influenced by $C_l = 0$ and $C_d = 0.5$ at the root and do not match design C_l and C_d.

Other BEM-calculated characteristics can be seen below, adding to the validation of Turkispain's rotor design.

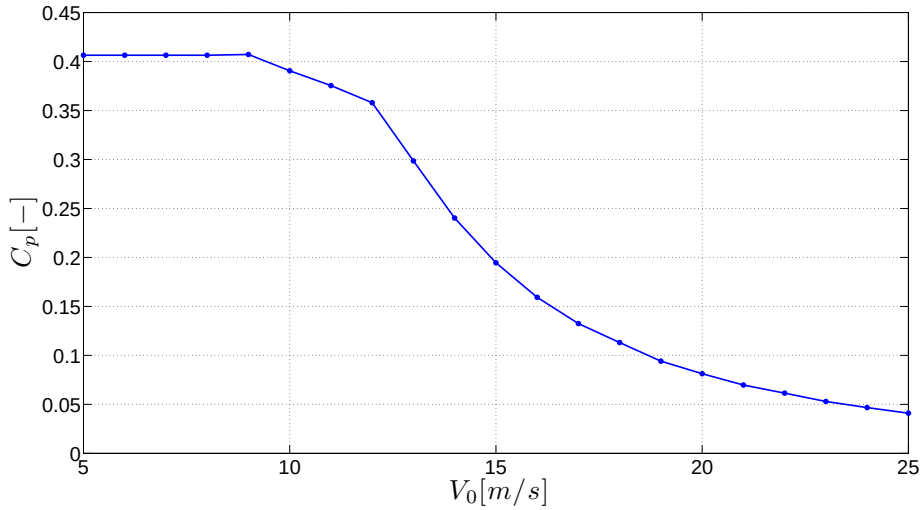

Figure 2.30: BEM C_p as a function of wind speed.

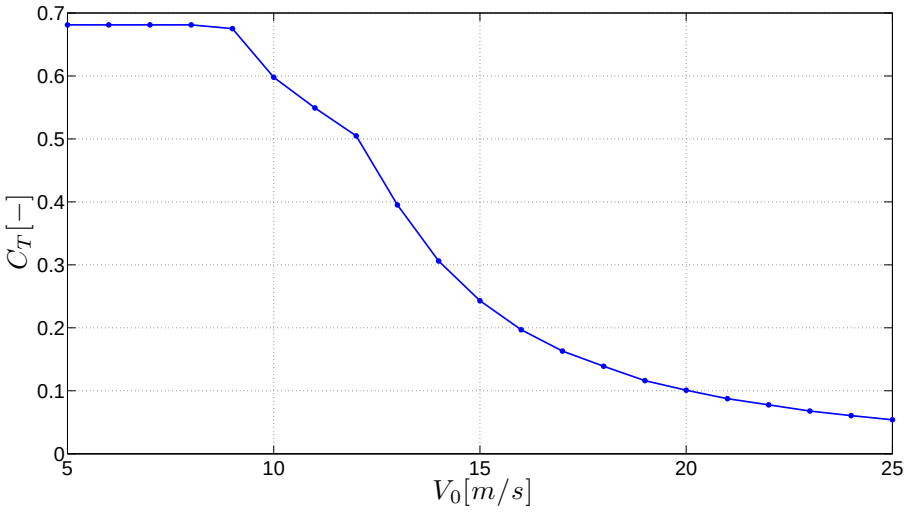

Figure 2.31: BEM C_T as a function of wind speed.

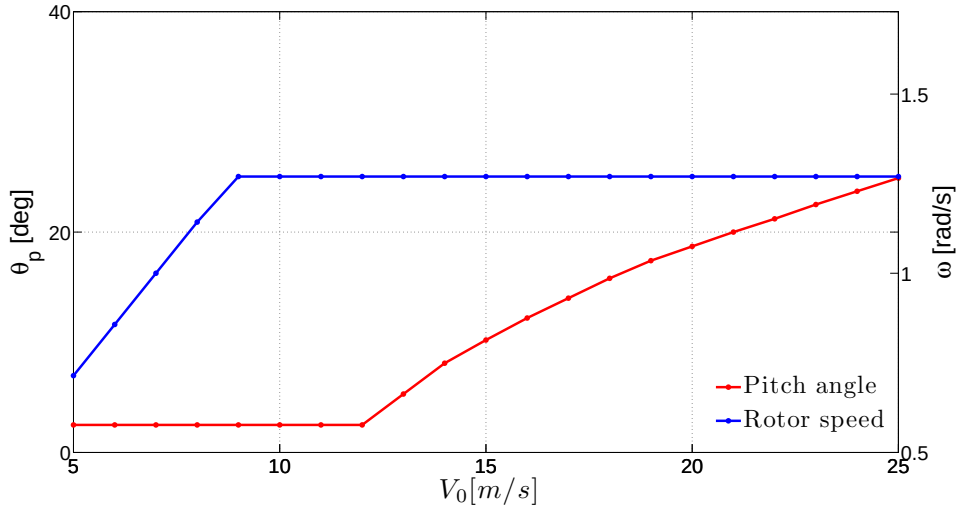

Figure 2.32: BEM Pitch angle and rotor speed as a function of wind speed.

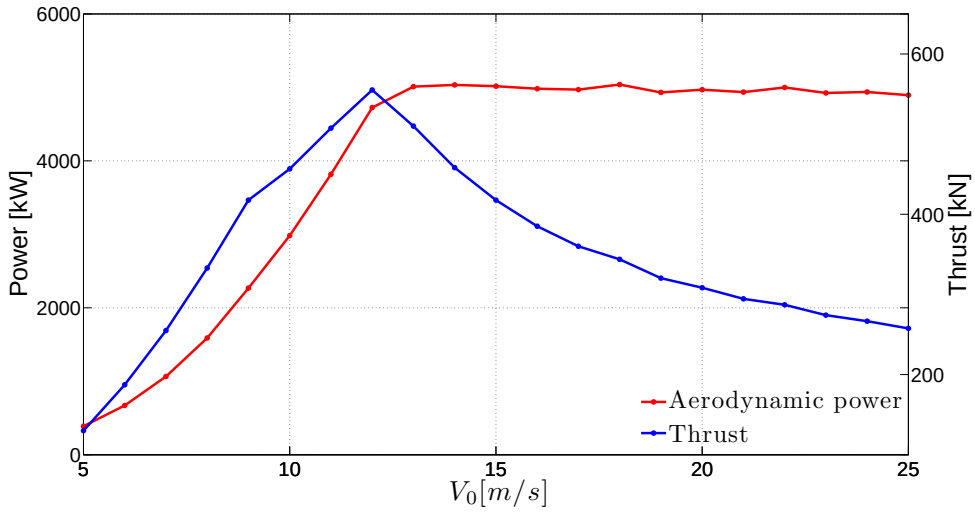

Figure 2.33: BEM Aerodynamic power and thrust as a function of wind speed.

The explanation as to why figure 2.32 shows a 2.5° pitch angle until rated wind speed lies on figure 2.34. Here, it can be seen that in order to stay in the safe range and avoid stall, a reasonable minimum pitch angle value is 2.5° because, from figure 2.34, the angle of attack along the blade for optimum $-2°$ is perhaps too close to the stall angle for all airfoils (which is around 10°, as seen in figures 2.5 to 2.8.

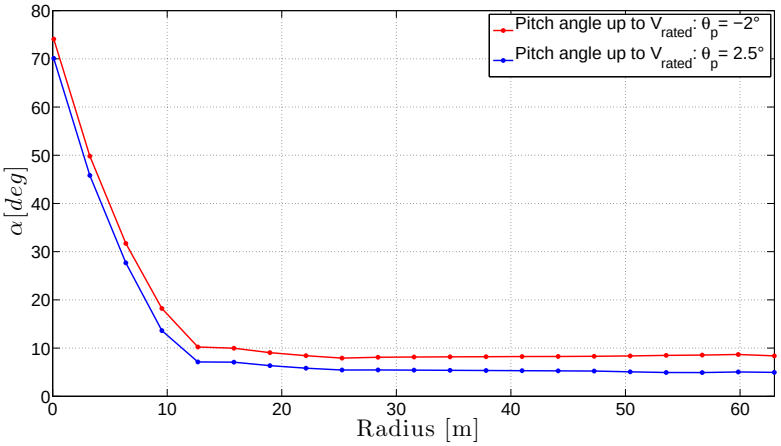

Figure 2.34: Angle of attack for different pitch angles until rated wind speed.

The drop in C_p when using a 2.5° pitch angle versus the optimum $-2°$ can be seen below.

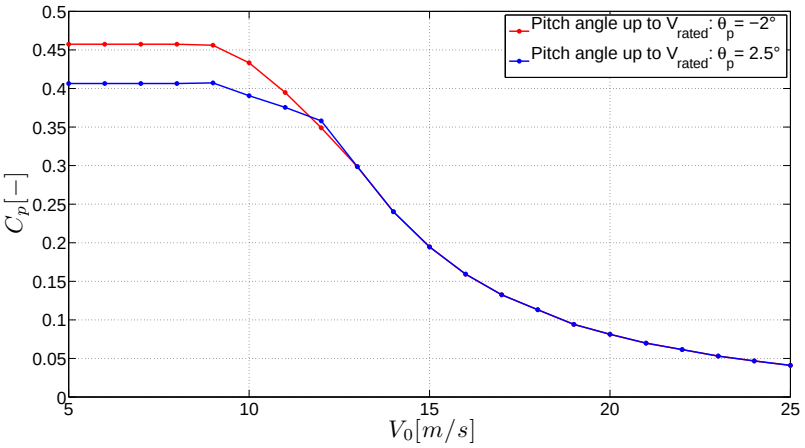

Figure 2.35: C_p for different pitch angles until rated wind speed.

Chapter 3

Structural blade design

This structural design part of this work has a simplified approach, i.e. real manufacturing issues (such as the design of joints), transportation difficulties etc. are neglected. Nevertheless, simplified Turkispain's blade structural design is, all the key decisions of the design process are explained in detail.

3.1 Blade design

3.1.1 3D envelope

The first part of the structural design of the blades is to build the 3D envelope. In order to do this, all that is needed is the relative thickness, chord and twist distributions obtained from the aerodynamic design process.

The first step towards a tridimensional construction, however, is a 2D process involving the airfoils outputted by the aerodynamic design, according to the relative thickness distribution (2.14). These shapes can be seen in figure 3.2. The rest of the airfoils are interpolations of the four originally chosen ones. It can be seen that there is a perfect circle at the root. The appropriateness of adding a tubular root part was discussed and finally accepted. As mentioned in the previous section, it was considered structurally inefficient to have an airfoil-shaped blade also at the root compared to having a purely tubular piece in the first 4 or 5 meters.

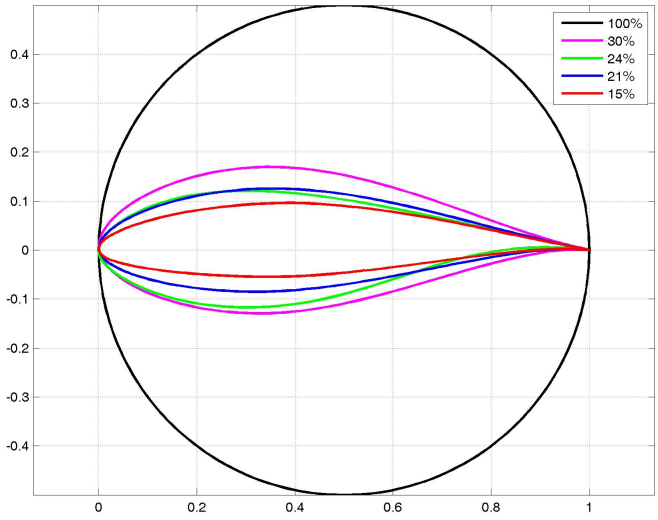

Figure 3.1: Main airfoils

In order to make a linear interpolation between the airfoils and obtain one airfoil per radial section, as seen in figure 3.2, the airfoil shapes were first re-discretised to 301 points and mirrored on the y axis.

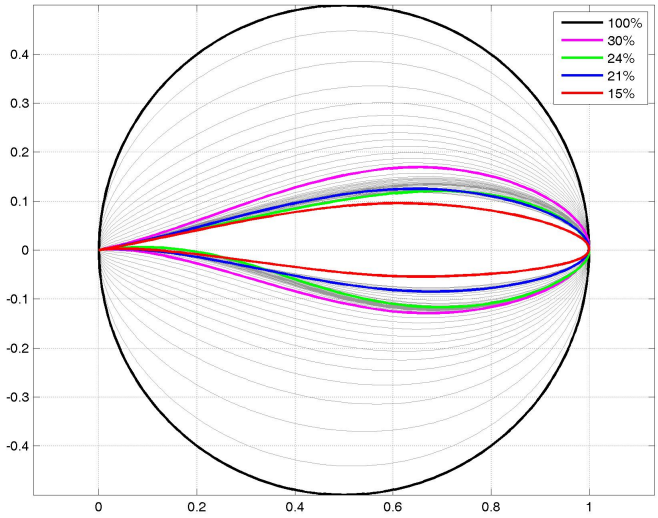

Figure 3.2: Interpolated sections.

Next followed to re-scale the airfoils at each section with respect to the chord distribution, fixing a point at the trailing edge as can be seen from figure 3.3.

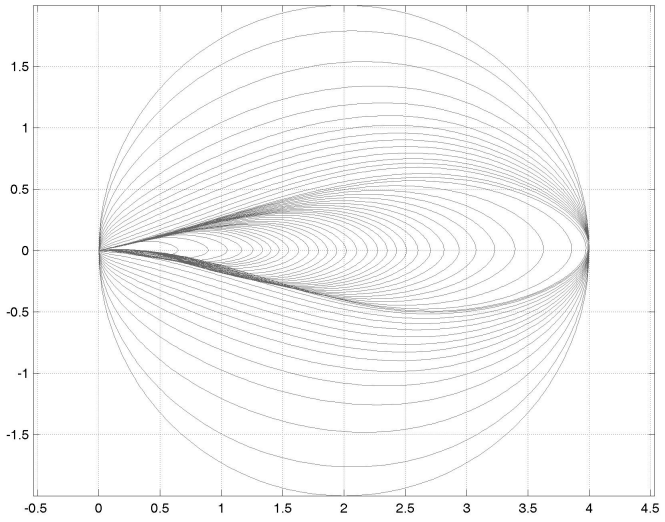

Figure 3.3: Scaled airfoil sections with fixed trailing edge.

Before applying the twist, each section was shifted in the x axis, so that the x coordinate of each airfoil, at which the thickness is largest, now stands at the origo. This choice was done so that each section can be twisted (rotated) about the point where its thickness is largest. *This is the same axis about which the blade will eventually be pitched.*

However, this procedure alone yielded a 3D envelope with surface indentations in the leading and trailing edges because the thickest section of the airfoils were not at the same chord percentage. In order to solve this problem, a smoothing filter was applied to the leading edge coordinates. The result of this can be seen in figure 3.4.

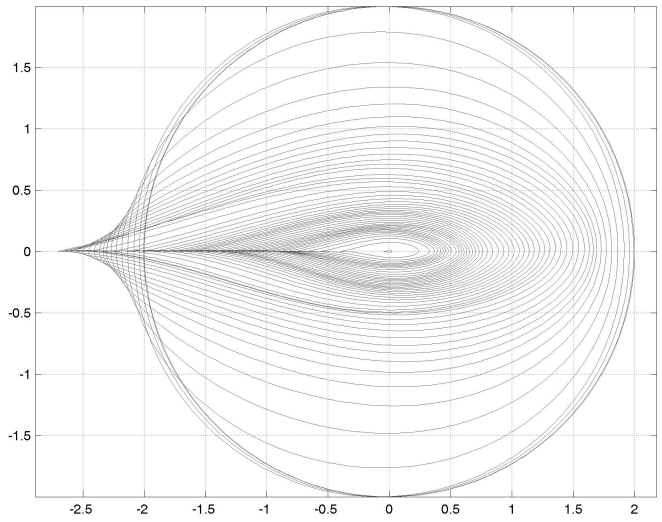

Figure 3.4: Alignment of sections without twist

After the process of alignment, twist was finally applied to all radial sections, according to the twist distribution outputted by the aerodynamic design process (2.14). Each section's airfoil was thus twisted about the twist/pitch axis, as seen in figure 3.5, where some aligned airfoils depict an initial sketch of Turkispain's 3D blade.

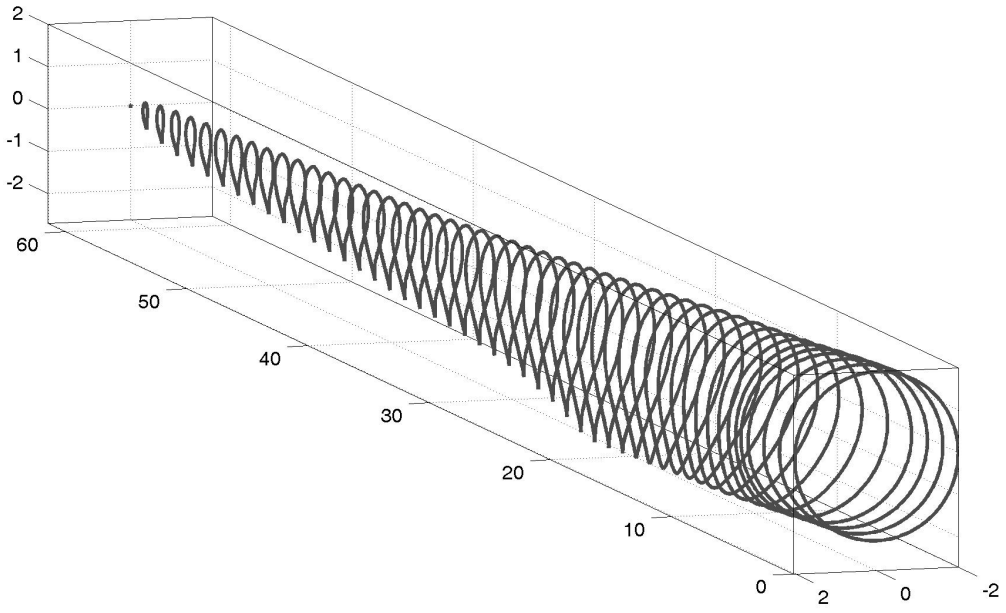

Figure 3.5: 3D blade sections with twist

The blade now looks sliced: it comprises 50 airfoils placed next to each other. Only 3 of them are the originally chosen ones: NACA at $t/c = 21\%$, FFA at $t/c = 24\%$ and NACA at $t/c = 30\%$. As already mentioned, the NACA airfoil at $t/c = 15\%$ does not appear; the smallest relative thickness to appear in the blade is $t/c = 19\%$.

3.1.2 Structural design

The blade can be considered as a clamped beam, subject to bending, torsion and shear at all cross-sections. This design process comprises the following points.

- *Key point definition:* the laying of different mat types needs a region definition for each section of the blade (each airfoil). Thus, 9 points were chosen among the coordinate points of each sectional airfoil, and designated as key points, as specified in [Structural Design and Analysis of Wind Turbine Rotor Blades, Robert D. Bitsche, October 2012].
- *Shear web location:* a 2-shear web structure was chosen for Turkispain's blades. In order to keep the shear webs reasonably straight from root to tip, 2 sets of 2 parallel imaginary lines were drawn (upper and lower parts of the blade) from root to tip. The closest 4 coordinate points of each sectional airfoil to these 4 intersecting lines were thus designated as key points 3, 4, 6 and 7, as seen in figures 3.6 and 3.7. Moreover, these 4 key points lie at the section where the thickness is largest, for all airfoils.

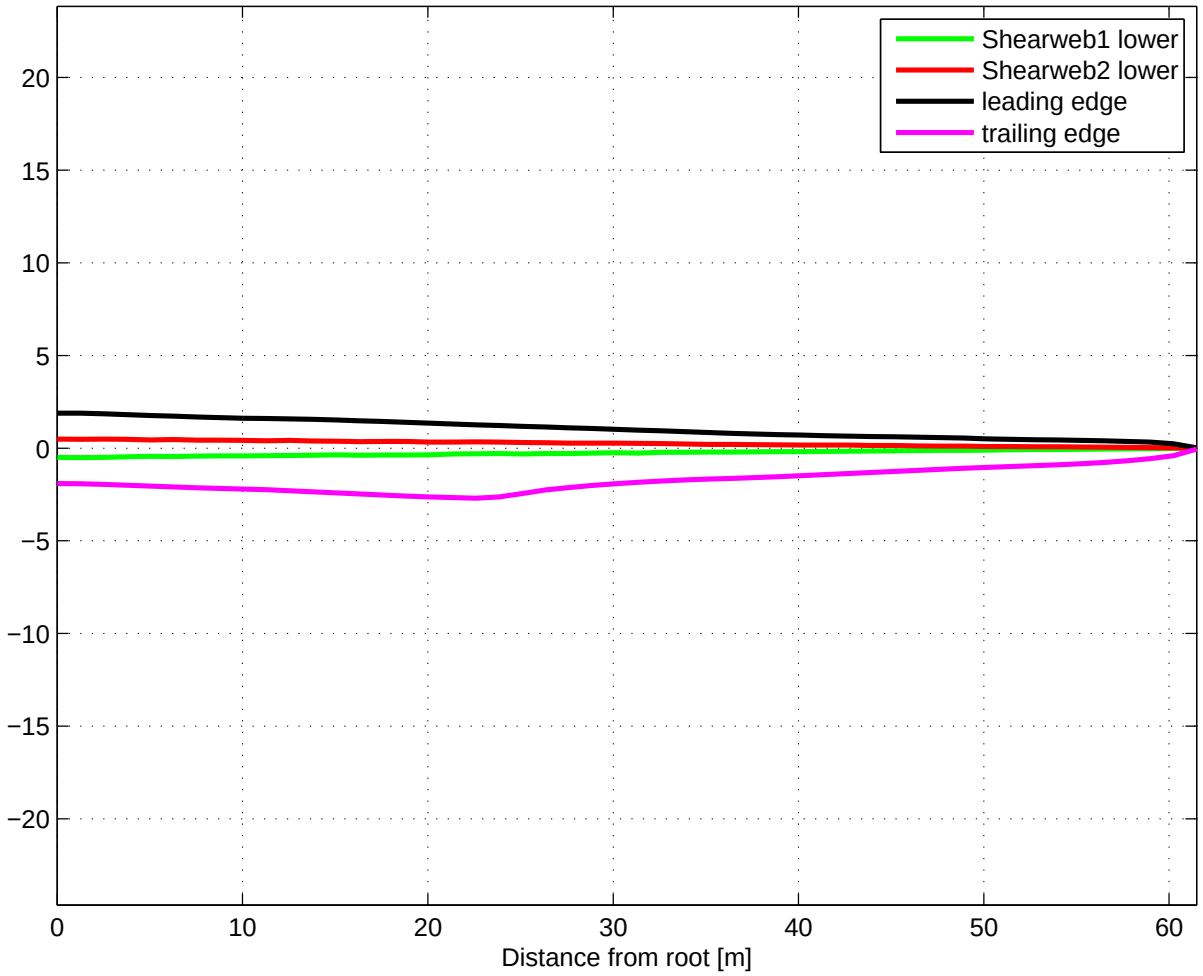

Figure 3.6: Lower part of the blade with shear webs

The 3D blade and some key point positions can be seen in figure 3.7.

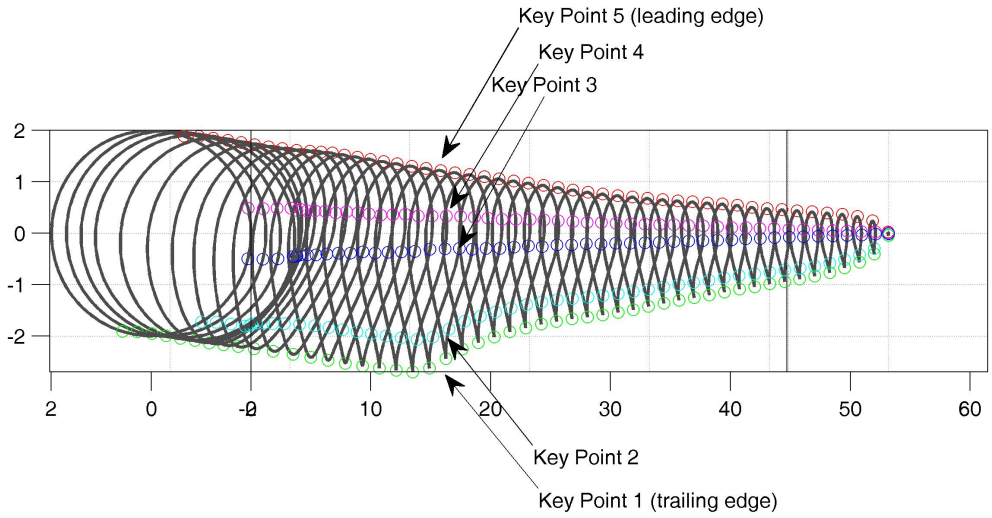

Figure 3.7: 3D blade sections with keypoints

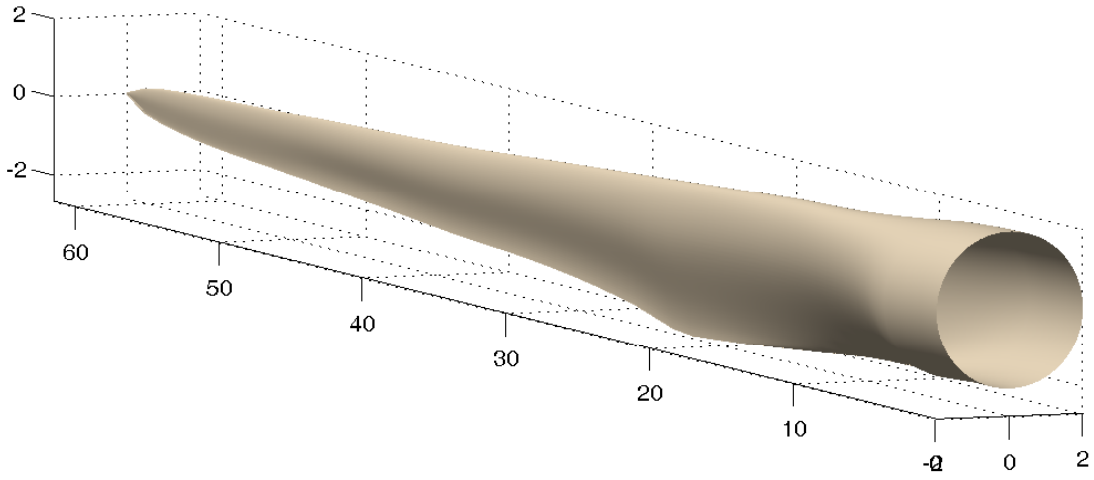

Figure 3.8: 3D blade view

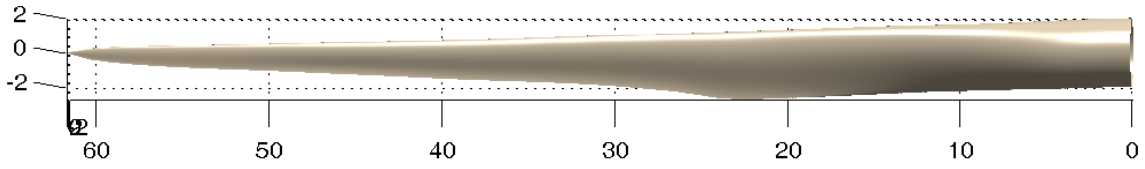

Figure 3.9: 3D blade view from side

- *Laying of mats:* provided the material characteristics are known, it can be determined, for each cross-section, which region needs what sort of material (the different regions are defined by the key points, as mentioned earlier). Figure 3.10 shows a sample cross-section of a blade.

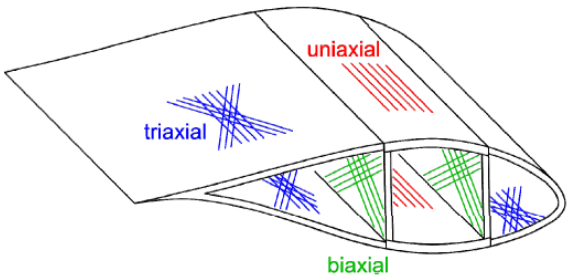

Figure 3.10: A cross section sketch with material type distribution. [Structural Design and Analysis of Wind Turbine Rotor Blades, Robert D. Bitsche, October 2012].

A brief description is added for the material type distribution of some cross-section:

- *Spar caps:* long, slender structures such as blades are subject to one directional stress along the spar caps (tension on the upwind side+compression on the downwind side). For this reason, the uni-axial fibres are located in the spar caps. Uni-axial fibres were chosen because the first Young Modulus of the uni-axial fibre material is fairly higher than that of the bi-axial or tri-axial materials, i.e. ($E_1 = 40\ GPa, E_1 = 12.4\ GPa, E_1 = 21.8\ GPa$, respectively).
- *Shear webs:* on the other hand, the shear webs are subject to shear forces, and their purpose is to prevent the spar caps from sliding (shearing). This results in a demand of bi-axial fibres in this region, which means they will intersect the spar cap fibres with 45° angle.
- *Trailing and leading edges:* the regions where most of these properties are required in a moderate level, hence the choice of tri-axial fibre material. In addition to fibres, core materials are laid to the leading edge, shear webs and towards the trailing edge. Core materials are used to save weight, stiffen and thicken laminates. And also they are fairly good at buckling prevention.

Choosing the thickness of the material is a more complicated process. Firstly, it is known that the biggest contribution to the blade mass stems from the spar caps, the region where the lift forces are effective and consequently flapwise bending moments are present. The thickness is increased in order to withstand this flapwise bending moment. However, this results in undesirably high edgewise bending moments which are mainly caused by the weight. (See figure 3.11).

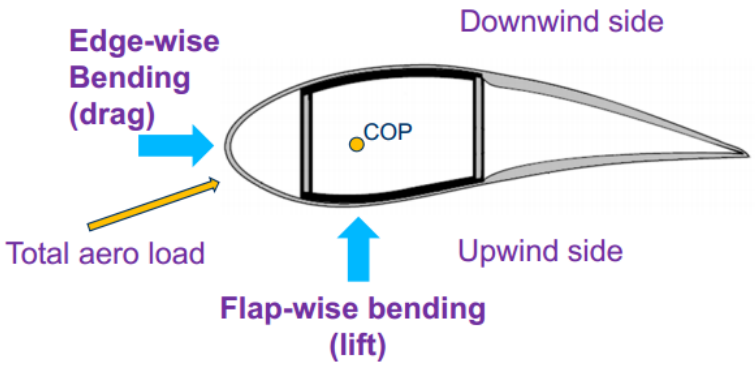

Figure 3.11: A cross section sketch with loading directions [Structural Design and Analysis of a 10 MW Wind Turbine Blade, Kevin Cox, Deep Sea Offshore Wind RD Seminar, 2012.]

In this work, the thicknesses of the spar caps, at each section, were determined by considering:

- The flapwise bending moment distribution along the blade corresponding to a 12 m/s incoming wind speed with a safety factor.
- A failure strain value.

The bending moment distribution was obtained from a BEM code, and the failure strain is known to be 0.3 % for FRPs: [Failure Criteria in Fibre Reinforced Polymer Composites: The World-Wide, M. J. Hinton A. S. Kaddour, Elsevier, 2004]. In order to follow this approach, however, it was assumed that, at each cross-section, the spar caps mimic an I beam. For each airfoil:

$$\varepsilon = \frac{M\frac{h}{2}}{IE} \tag{3.1}$$

where ε is the strain, M is the BEM-calculated bending moment along the blade, h is half the airfoil thickness, E is the Young Modulus and I is the moment of inertia. Since the aim is to determine the thicknesses of the layers, and since the spar caps are the main region the forces are acting on, the shear webs were ignored when calculating the area. This area, A, is thus:

$$I = Ah^2 \tag{3.2}$$

where

$$A = 2\delta l \tag{3.3}$$

δ being the desired spar cap thickness, l the spar width. (For the sake of simplicity, this width is assumed to be non-curved).

After manipulating these equations, δ can be expressed as a function of the radius of the blade, as seen in equation 3.4.

$$\delta(r) = \frac{M(r)}{2E\varepsilon lh} \tag{3.4}$$

As mentioned, in order to obtain the moment distribution along the blade, a simple BEM code was executed for a case where the wind speed is 12 $\frac{m}{s}$, without pitch. This is the rated speed with no pitch. In addition, in order to

be in a safe range and other considerations which will be elaborated later on (stiffness,mass distribution etc.) these values were multiplied with a safety factor of 2 .In the fig. 3.12 this is depicted.

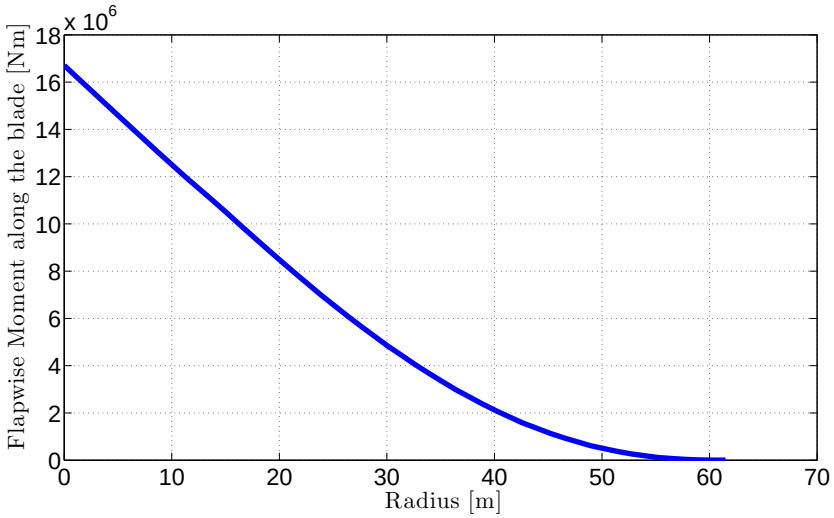

Figure 3.12: BEM results for flapwise moment distribution along the blade (WS = $12\frac{m}{s}$)

Apart from determining the spar cap thickness for each section, all cross-sections were scaled by assigning a reference chord to the sample cross section input (specified in the sample BECAS code handed out by Robert Bitsche). Because the moment approach was more reliable than assigning a random reference chord throughout the very first visual inspections, the thicknesses were compared with respect to that. After visual inspection, a plausible reference chord value range was determined ([0.7 - 4]). A more detailed tuning was done for the reference chord by checking the eigen-frequencies from HAWCStab2 simulations (see table 3.2). After a few iterations, the reference chord is concluded to be **1.6 m**. The sample BECAS ouputs for the selected sections are depicted in figures 3.14 to 3.22.

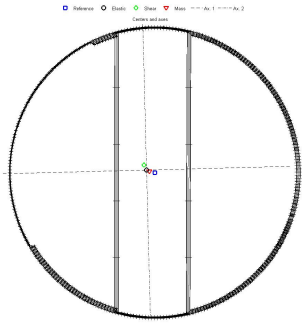

Figure 3.13: % 100 Thickness Airfoil Section Sample with centers

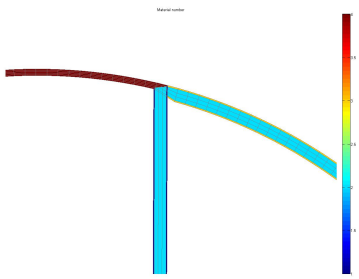

Figure 3.14: Zoomed view

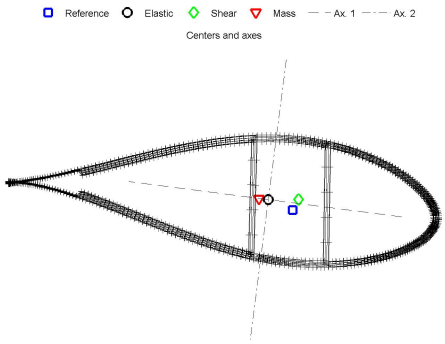

Figure 3.15: % 30 Thickness Airfoil Section Sample with centers

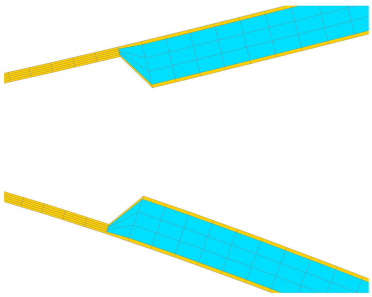

Figure 3.16: Zoomed view

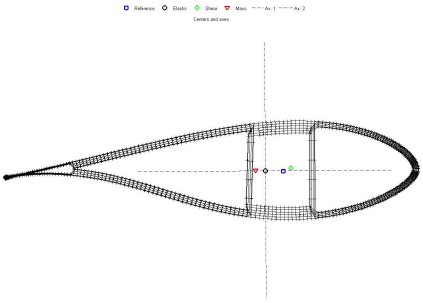

Figure 3.17: % 24 Thickness Airfoil Section Sample with centers

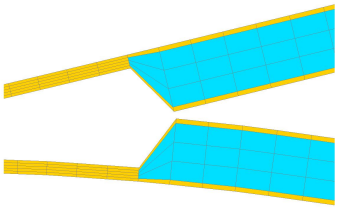

Figure 3.18: Zoomed view

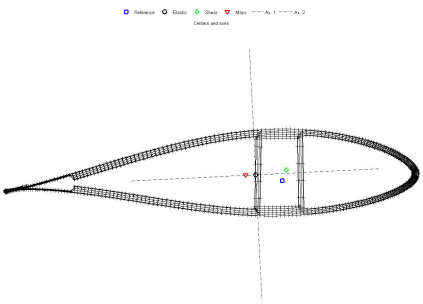

Figure 3.19: % 21 Thickness Airfoil Section Sample with centers

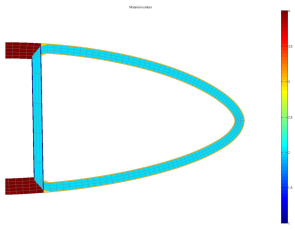

Figure 3.20: Zoomed view

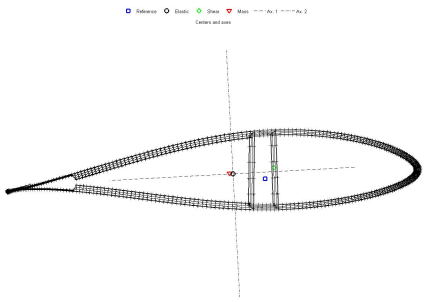

Figure 3.21: % 19 Thickness Airfoil Section Sample with centers

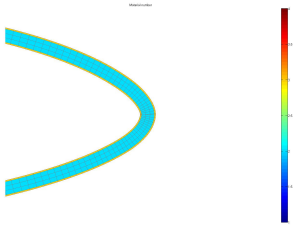

Figure 3.22: Zoomed view

Regarding the blade total mass: for each of the aforementioned reference chord iterations, a total blade mass was obtained. Once it was seen that the lower natural frequencies were in the reasonable range, the total mass of one blade was found to be:

$$M_{blade} = 15678\ kg \tag{3.5}$$

This mass is less than the two wind turbines which served as reference for this report, NREL 5MW and Areva Multibrid 5MW, as seen in table 3.1.

Blade total mass [kg]		
Turkispain 5MW	NREL 5MW	Areva Multibrid 5MW
15679	17740	16500

Table 3.1: Comparison of blade masses.

Also, from HAWCStab2 simulations it is possible to list the eigen-frequencies of the first 10 modes of vibration of Turkispain's blade, along with the logarithmic decrement (see table 3.2).

Eigenfrequency Type	Frequency [Hz]	Log Decrement [%]
1st Flapwise	0.81	1.75
1st Edgewise	0.96	3.50
2nd Flapwise	2.03	2.10
2nd Edgewise	2.68	2.45
3rd Flapwise	3.86	5.60
3rd Edgewise	5.78	3.20
4th Flapwise	6.38	5.80
5th Flapwise	9.40	6.40
4th Edgewise	9.86	7.03
1st Torsion	11.71	7.73

Table 3.2: Blades first 10 modes at stand still for Turkispain (HAWCStab2 output).

3.2 Hub design

The hub was modelled as a concentrated mass of $56780kg$ located in the last node of the shaft (node number 5). This mass is an exact copy of NREL's hub mass, which was, in turn, taken from REpower 5M. AREVA 5M was also inspected, for comparison purposes: its hub mass is $62000kg$, and so it was preferred to use REpower's mass. Since both reference turbines have a hub radius of 1.5 meters, this is the length assigned to Turkispain's hub radius. Furthermore, as was done in [Definition of a 5-MW Reference Wind Turbine for Offshore System Development, NREL Technical Report], assuming the hub as a thin spherical shell and also taking a radius of $1.75m$, the inertia of the hub can be calculated as in equation 3.6.

$$I = \frac{2}{3}mr^2 = \frac{2}{3} \cdot 56780 \cdot 1.75^2 = 115930 \; kgm^2 \tag{3.6}$$

Since the hub is a concentrated mass in the *.htc* file, the input masses per length are almost zero in the *.st* file. The Young Modulus, E, is $2.1 \cdot 10^{11} N/m^2$ for the flexible case and $2.1 \cdot 10^{17} N/m^2$ for the stiff case. Similarly, the shear modulus, G, is $8.08 \cdot 10^{10} N/m^2$ and $8.08 \cdot 10^{16} N/m^2$, respectively. The remaining *.st* file inputs were kept the same as in NREL's case.

3.3 Nacelle

The nacelle was also modeled as a concentrated mass, in this case located in the second node of the tower top main body. This corresponds to 90 meters above ground. REpower's mass for the nacelle is $240000kg$, and AREVA's is $233000kg$. They are relatively close values. Again, it was preferred to use REpower's mass of $240000kg$, since this was used for NREL. As for the inertia of the nacelle, it was calculated by assuming it to be a solid rectangular prism. Using Steiner's Theorem, the equation for the nacelle inertia about the yaw axis (located a distance r from the parallel axis crossing the center of mass) is:

$$I_{total\ nacelle} = I_y + mr^2 \tag{3.7}$$

where $I_y = \frac{1}{12} mass \cdot width \cdot length$.

The nacelle is assumed to be $4m$ in width, r is $1.9m$ and the length is estimated to be $5m$. When all these parameters are plugged in the inertia is found to be:

$$I_{total\ nacelle} = 1698000 \;\; kg \cdot m^2 \tag{3.8}$$

3.4 Drivetrain/shaft design/tower design

From tower top towards the rotor center 5 nodes are present. This distance is estimated as $5m$, as mentioned in the previous section. Taking the $5°$ of tilt angle into account, the total length becomes $\frac{5}{cos(5)} = 5.0191m$. The main bearing is located at $3.11m$.

There is another concentrated mass in the first node of the shaft, which represents the generator equivalent slow shaft. Here, the input inertia value was tuned with respect to the output of the HAWCStab2 simulation for the controller. Eventually, a generator inertia of $30999000kg \cdot m^2$ was used. The rated shaft speed was calculated as in equation 3.9:

$$RPM_{rated} = \frac{V_{tip,max}}{R} = \frac{80}{63} = 1.26 \; rad/s = 12.12 \; rpm \tag{3.9}$$

Where $V_{tip,max} = 80m/s$ is the maximum design linear tip speed, $R = 63m$ the radius from the rotation center up to the tip.

Apart from these bodies, the tower properties were kept the same as NREL's. Since the rotor diameter of Turkispain is also $126m$, upscaling was not required. The tower comprises 8 nodes as one main body up to 87.6 meters instead of 90, since there is an extra main body *towertop*. In the literature, it was found that the total mass of 65-70 meters tubular steel towers were in the range of 230 to 270 tonnes [Wind Turbine Towers Establish New Height Standard, US DOE Technical Report, 2010]. The total mass of Turkispain's tower has been calculated by integrating the masses per length in the *.st* file input over the total length. This results in a plausible value. However, a more in depth investigation is conducted in the following section, showing that a new design of the tower was required.

$$Tower\ Mass = 347460\ kg \tag{3.10}$$

3.5 Initial check of aeroelastic model

With all these above mentioned inputs (structural *.st*) plus the aerodynamic properties (*.ae*,*.pc*)), HAWCStab2 simulations were performed in order to get the stand still eigenfrequencies. In additon, since the1P range was already known by inputting the highest and lowest angular speeds, it could be checked if there was any undesired intersection of the frequencies. Indeed, in this case, the tower frequency was intersecting the 3P for low rotational speed (see figure 3.23). By observing this, it was concluded that a tower redesign was required. This is also advantageous from the manufacturing point of view: using less material for the tower lowers the expenses.

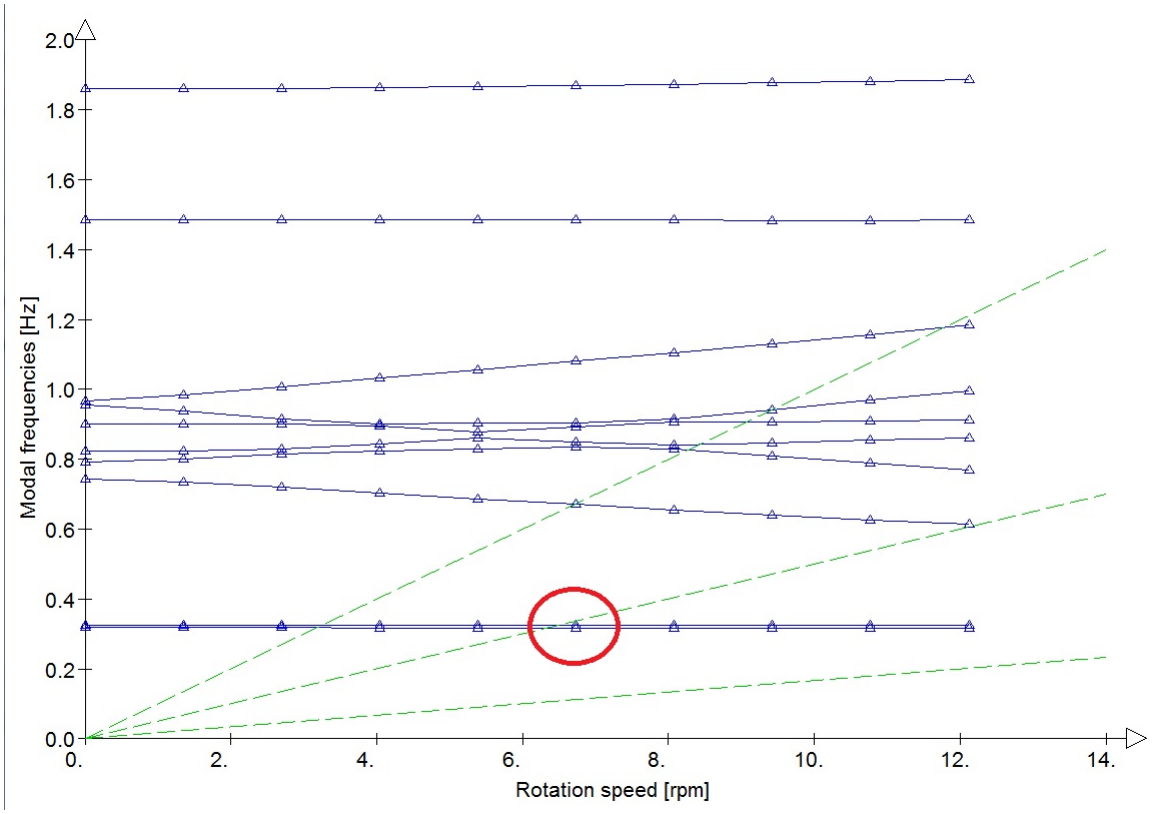

Figure 3.23: A screenshot from HAWCStab2 modal analysis for the entire turbine

Apart from this, also the tip deflection values were inspected via the same simulation. The tip clearence values were not sufficiently high and also a comparison for the same case with NREL 5MW reference turbine was conducted. The difference between the highest tip deflections was fairly high (table 3.3). It was thus concluded that prebending of the blades would help to avoid many possible problems (see section 3.6).

Turkispain without prebending	NREL
7.69 [m]	3.01 [m]

Table 3.3: Comparison of maximum tip deflections at 11 [m/s].

3.6 Re-design of the tower and prebending of the blades

- Re-design of the tower. For the re-design of the tower, the excel sheet was used. For simplicity, the height was not changed (87.6 meter excluding the tower top), but the thicknesses were altered. The new design output was plugged into the *.st* file. In order to make sure that this actually helped to solve the problem, another HAWCStab2 simulation was carried out. The frequency was lowered from $0.35Hz$ to $0.26Hz$. The new results are depicted in figure 3.24. The mass comparison is conducted. And also the new tower design with inner, outer diameters and thicknesses is given in table 3.11.

$$Tower\ Mass\ Comparison = Old\ Tower\ Mass - New\ Tower\ Mass = 347.460\ [kg] - 238.645\ [kg] = 109.000[kg] \tag{3.11}$$

Global height [m]	Outer diameter [m]	Thickness [mm]	Inner diameter [m]
0,000	8,000	26	7,94800
12,500	7,572	24	7,52390
12,501	7,572	24	7,52390
25,000	7,144	23	7,09780
25,001	7,144	23	7,09780
37,500	6,716	22	6,67180
37,510	6,715	22	6,67140
50,000	6,288	20	6,24770
50,001	6,288	20	6,24760
62,500	5,860	18	5,82360
62,501	5,860	18	5,82360
75,000	5,432	17	5,39750
75,001	5,432	17	5,39750
87,600	5,000	16	4,96800
87,601	5,000	16	4,96800

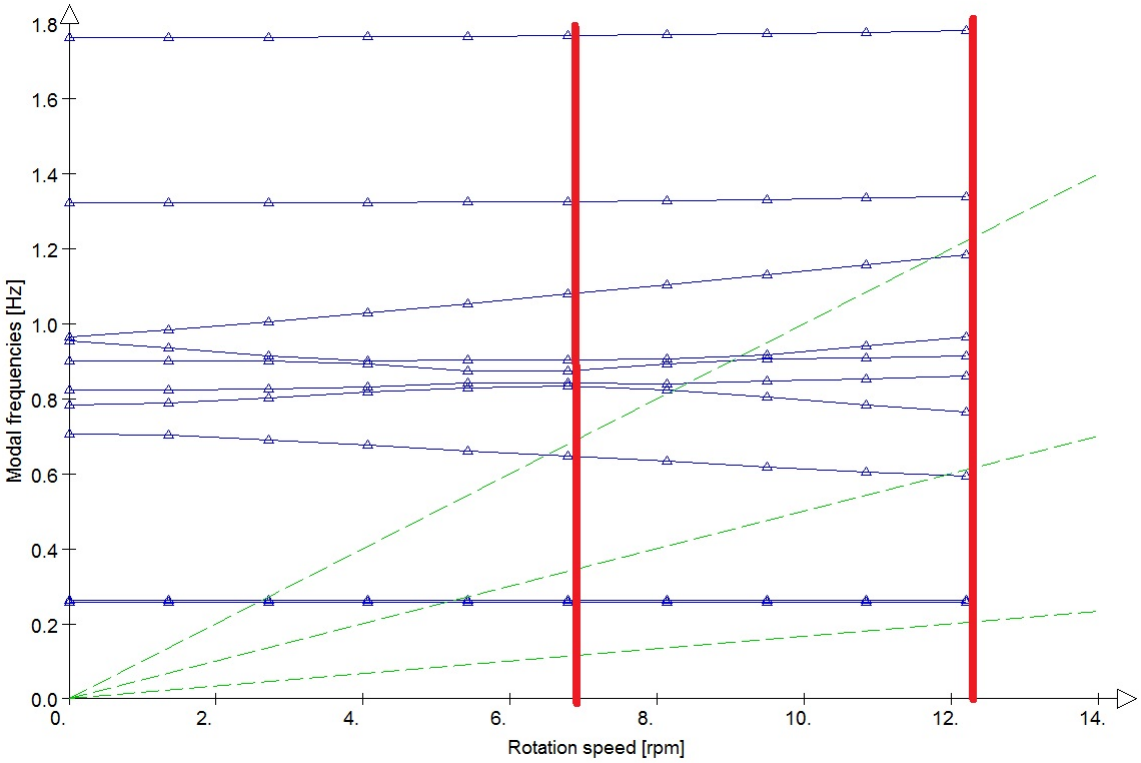

Figure 3.24: A screenshot from HAWCStab2 modal analysis for the entire turbine after redesigin of the tower

- Prebending of the blades ; This is quite commonly used in current design of wind turbine blades. It not only provides a larger swept area during operation, but it also increases the tip clearence. However, the reason that prebending is applied on Turkispain's blades is the fact that before prebending the tip deflections were too high. Overall, this results in a torsion on the blades. To avoid the problem, the tip deflection amount for 8 m/s was taken as a reference and thus, the *.htc* file was modified. The blades were hence prebent. The comparison for the maximum tip deflections was redone, see table 3.4. This was a satisfactory value for such long blades and also the tip clearence was checked.

Turkispain with prebending	NREL
4.11 [m]	3.01 [m]

Table 3.4: Comparison of maximum tip deflections at 11 [m/s] with prebending on Turkispain.

Chapter 4

Implementation of PI Controller

The HAWC model is equipped with an interface for control systems through a Dynamic Link Library (DLL) format [Control Design for a Pitch Regulated, Variable Speed Wind Turbine, M H. Hansen, A. Hansen, T. Larsen, S.ye, P. Srensen, P. Fuglsang, Ris-R-1500(EN), 2005]. This interface enables the control of the turbine via a pitch angle and a generator torque from a control program outside the HAWC core. The main idea of the DLL is to divide the control unit into different procedures that can be called by HAWC:

- The first procedure is the regulator, which basically consists of the controlling algorithm of the pitch and power references.
- The second procedure is the pitch servo algorithm, which calculates the transient position of the pitch angles between the pitch angle set points.
- The last procedure is the generator subroutine, which calculates the generator mechanical torque transient corresponding to the rotational speed of the generator and the reference electrical power. This enables variable speed control through active power setting. [Description of the DLL Regulation Interface in HAWC, T. Larsen, Ris-R-1290(EN), 2001].

After quoting briefly what the background of the used controller is like, the main three regions are elaborated. The main goal of the controller is to optimize the power production below rated wind speed and limit power and loads at high wind speeds. This is done via adjusting the pitch angles and the generator torque according to the measured rotational speed [Comparison between a PI and LQ-regulation for a 2 MW Wind Turbine, N. Poulsen, T. Larsen, M. H. Hansen, Ris-I-2320(EN), 2005].

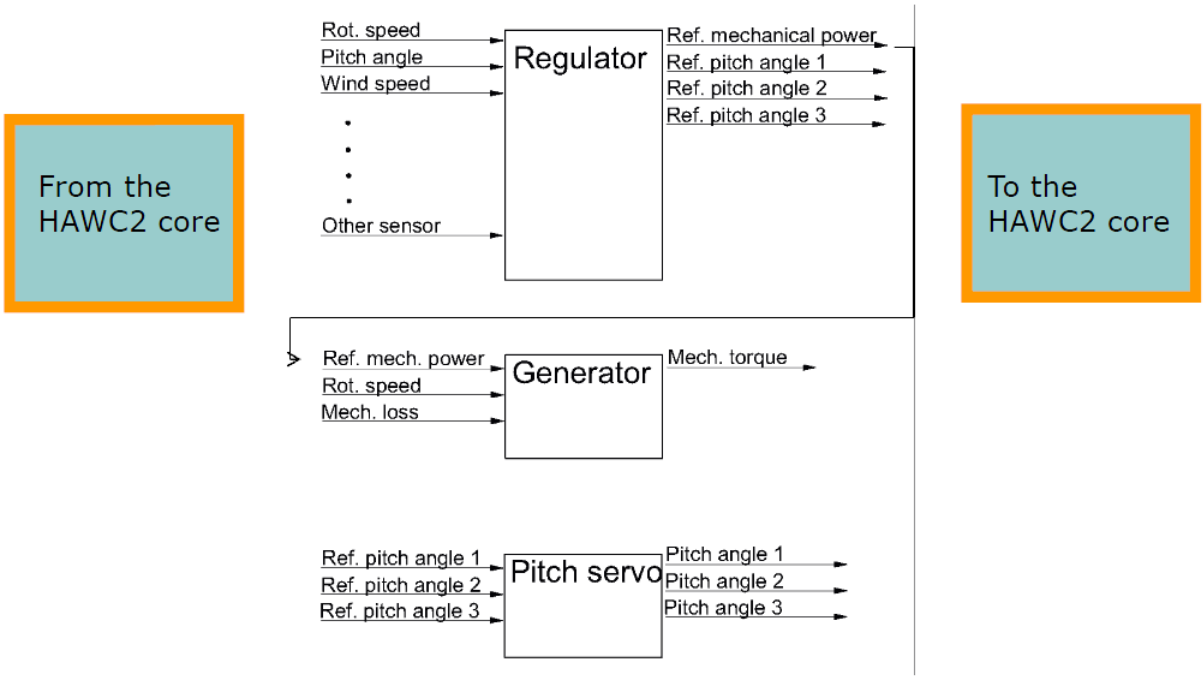

Figure 4.1: Principle of control through an external DLL [Source: Lecture Slides Week 8, M. H. Hansen, 2012]

It follows to overlook the purpose and behaviour of the controller for all three regions of the turbine operational range.

- **Region 1** : Optimal C_p is sought for by keeping an optimal pitch and by using the generator torque in order to obtain an optimal tip speed ratio. In other words, in this region, the aerodynamic torque is in balance with the generator torque. (Equation 4.1).

$$Q_{generator} = K\Omega^2 \quad where \quad K = \eta \frac{0.5\rho A R^3 C_p(\lambda opt, \theta_{opt})}{\lambda^3} \tag{4.1}$$

  The value for this optimal-C_p-tracking factor is, as outputted by HAWCStab2, $K = 0.829 \cdot 10^6 \frac{kNm \cdot s^2}{rad^2}$

- **Region 2**: This is the region where generator torque is effective on the regulation of the rotor speed when taking rated rotor speed into account. The generator torque is set with respect to the PI feedback, which calculates the speed error.

$$\Delta Q_g = k_p g \dot{\phi} + k_I g \ddot{\phi} \quad where \;\; (\Omega - \Omega_r) = \dot{\phi} \tag{4.2}$$

  Considering equation 4.2, the simplified equation of motion of the drive-train is:

$$(I_r + n_g^2 I_g)\ddot{\phi} + \frac{1}{\eta} k_p g \dot{\phi} + \frac{1}{\eta} k_I g \phi = 0 \tag{4.3}$$

  The eigenvalues of equation 4.3 give the required gain factors. This analysis was conducted in HAWCStab2. The results for these can be seen below. In addition, the generator inertia obtained from HAWCStab2's results were plugged into the main *.htc* command file, since these gain factors correspond to such inertia value.

$$Proportional\ gain\ of\ torque\ controller = k_pg = 0.257 \cdot 10^8\ \frac{Nm \cdot s}{rad}$$
$$Integral\ gain\ of\ torque\ controller = k_Ig = 0.115 \cdot 10^8\ \frac{Nm}{rad}$$
$$I_g = 30999000\ kg \cdot m^2$$

- **Region 3**: In this is region, the blades are effectively pitching in order to control the rotor speed, whilst the generator torque is being used to regulate the power. Since the generator torque can be changed much faster than the pitching of the blades, it is still in the play in this regulating scheme. Apart from this, there is another factor which is basically left for the manufacturer to make: either constant power or constant torque. In the design process of Turkispain, constant power was chosen. This means that the generator torque is defined as $\frac{P_r}{\Omega}$. Analogously to the second region, there is a PI feedback from the speed error. However, this time it is fed into the pitch angle.

$$\theta = k_p\dot{\phi} + k_I\ddot{\phi} \quad where(\Omega - \Omega_r) = \dot{\phi} \tag{4.4}$$

Considering equation 4.4, the simplified equation of motion of the drive-train is:

$$(I_r + n_g^2 I_g)\ddot{\phi} + (\frac{1}{\eta}\frac{dQ_g}{d\Omega} - \frac{dQ}{d\theta}k_p)\dot{\phi} + \frac{1}{\eta}k_I\phi = 0 \tag{4.5}$$

The eigenvalues of this give the required gain factors. This analysis was conducted in HAWCStab2. The results for these two can be seen below.

$$Proportional\ gain\ of\ pitch\ controller = k_p = 3.54\ \frac{rad \cdot s}{rad}$$
$$Integral\ gain\ of\ pitch\ controller = k_I = 1.59\ \frac{rad}{rad} \tag{4.6}$$

As seen from equation 4.6, the aerodynamic torque gradient is a fairly important parameter. This was calculated via HAWCStab2 as well. Figure 4.2 shows a linear fit to the gain and the turbine's response with respect to the pitch angle. The coefficient of linear term in the aerodynamic gain scheduling was found to be 4.74°.

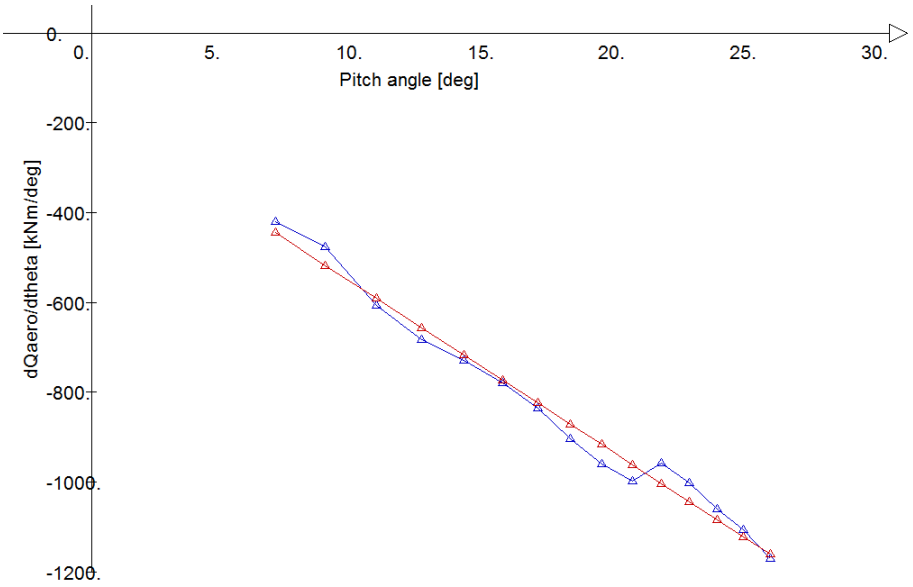

Figure 4.2: HAWCStab2 Result for the aerodynamic torque gradient vs pitch.

In addition to these tuned values, other parameters were also tweaked with respect to Turkispain's characteristics:

- *Minimum pitch angle and rated rotor speed:* The rated rotor speed is 1.26 rad/s (calculated as in equation 3.9), however only 60 % of this value was plugged in as the minimum rotor speed, i.e. 0.76 rad/s. The optimal operational pitch and rotor speed were calculated via HAWCStab2 (this was also obtained from a simple BEM code, as was seen in the aerodynamic design section). The plot is depicted in figure 4.3.

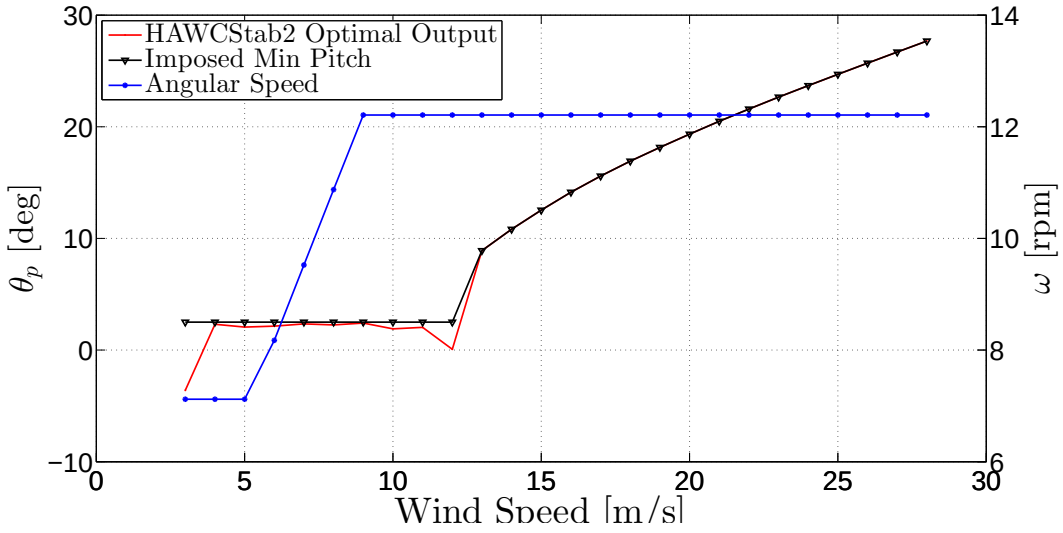

Figure 4.3:

In order to stay in the safe range and avoid stall, the minimum pitch value was chosen as 2.5 degrees. This choice was justified in figure 2.34 in the Aerodynamic Design section, where it was seen that the angle of attack along the blade, for $-2°$, was perhaps too close to the stall angle for all airfoils (which is around $10°$).

- *Maximum allowable torque.* It is known that torque is power divided by rotor speed. In this case, this is rated power divided by rated rotor speed. This quantity was multiplied by a safety factor of 1.4, as seen in equation 4.7.

$$\begin{aligned} Maximum\ \ Allowable\ \ Generator\ \ Torque &= 1.4 \cdot Rated\ \ Torque \\ 1.4 \cdot \frac{5000000}{1.26} &= 1.4 \cdot 3928571\ Nm = 5.5 \cdot 10^6\ Nm \end{aligned} \tag{4.7}$$

- *Free-free drive train torsion frequency and frequency of the generator speed filter.* The DT torsion frequency was found via a HAWCStab2 simulation where the bearing was set to be free (i.e. bearing 1) and the modal analysis for the whole turbine was simulated. By determining the correct mode, the frequency value was obtained. Half of this value was plugged in as the generator speed filtering frequency. This is important in order to decrease response at the free-free drive train frequency. This filter makes sure that any torque demand at the free-free frequency is in counter phase before entering the structural model.

$$\begin{aligned} Free - Free\ \ Drive\ \ Train\ \ Torsion\ \ Frequency &= 0.91\ Hz \\ Frequency\ \ of\ \ generator\ \ speed\ \ filter &= 0.45\ Hz \end{aligned} \tag{4.8}$$

Chapter 5

Aeroelastic analysis

5.1 Fatigue

The main goal is to decrease the cost of energy. One way of doing this is to lengthen the lifetime of the turbine as much as possible, and fatigue is thus a decisive factor to look into. The IEC standards contain specific load cases that a turbine has to withstand, but only an abbreviated version of such cases was simulated for this section. All these simulations were done for a period of $600s$.

The idea of such a procedure is, for each load case, to calculate the equivalent load value that would cause the turbine to suffer as much fatigue damage as would have been 20 years. The fatigue damage was calculated via the Rainflow Counting method. Thus, the procedure used is:

- The DLCs were simulated for Turkispain.
- The load processes were extracted (e.g. tower lateral bending moment, blade edgewise bending moment).
- For a given wind climate (see chapter 6), the corresponding hours are fed in, such that from the total hours in a 20-year period, half were with no yaw error, a quarter with $10°$ of yaw error, and a quarter with $-10°$ of yaw error.
- All these signals were transformed to half and full cycles via the Rainflow method for corresponding bin widths of moments (kNm).
- 10 million cycles were picked, which corresponds roughly to a 20-year use of a wind turbine.
- The material characteristics, m, was chosen correspondingly. m is the slope of the Wöhler Curve. In this analysis, these values were 10 and 4 for the blades and the steel, respectively.
- The same procedure was implemented for NREL for comparison purposes.

All these equivalent loads, for the chosen load processes, are listed in table 5.1, where it is clear that Turkispain's equivalent loads, for the same wind climate and for 20 years, are less than NREL's.

In addition, a similar analysis was conducted, this time in order to observe the relation between wind speed and equivalent loads. It is known that equivalent loads are supposed to increase with increasing wind speed; many of the plots below agree with this, with some exceptions (these exceptions are where normally the second main iteration starts for the turbine designer). In the cases where the equivalent loads are higher at a lower wind speed, this is very likely caused by undesirable resonances. However, due to time limitations, a deeper investigation was not conducted. (Figures from 5.1 to 5.11.)

Equivalent load [kNm]		
Load process	Turkispain	NREL
Tower bottom longitudinal moment (Mx)	27508.20	37593.12
Tower bottom lateral moment (My)	11311.00	17557.95
Tower yaw moment (Mz)	8510.64	9360.15
Main shaft bending moment (Mx)	11624.87	12400.69
Main shaft bending moment (My)	11689.65	12415.69
Blade root flapwise bending moment Blade 1 (Mx)	9073.55	9385.22
Blade root edgewise bending moment Blade 1 (My)	7988.83	9309.58
Blade root flapwise bending moment Blade 2 (Mx)	9037.11	9610.89
Blade root edgewise bending moment Blade 2 (My)	8001.49	9332.20
Blade root flapwise bending moment Blade 3 (Mx)	9024.41	9474.71
Blade root edgewise bending moment Blade 3 (My)	7988.19	9351.11

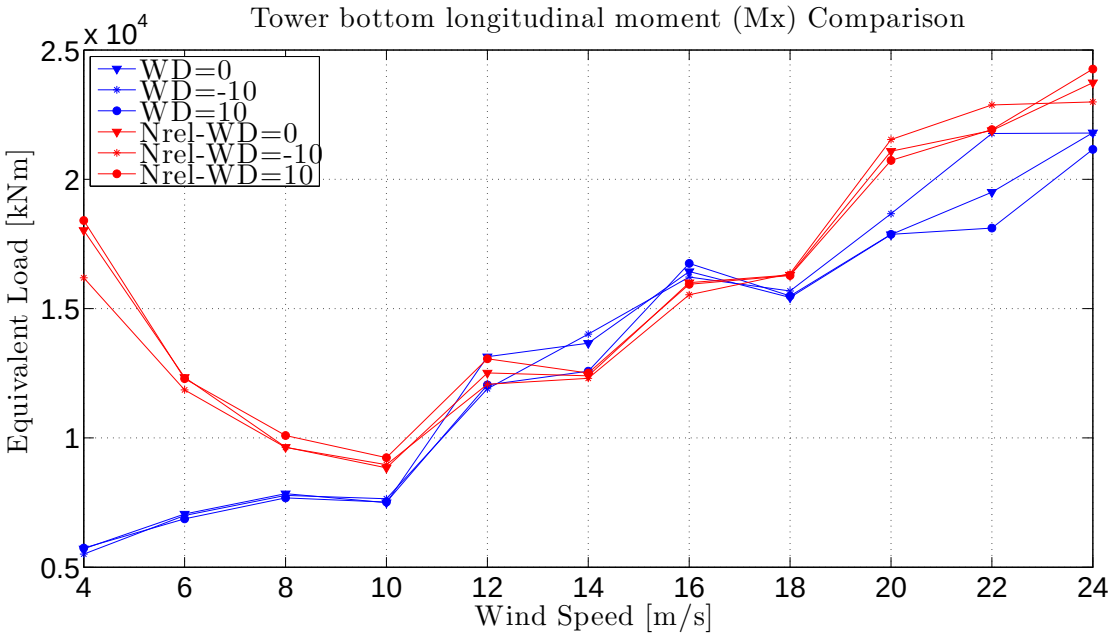

Figure 5.1: Tower bottom longitudinal moment (Mx) Comparison

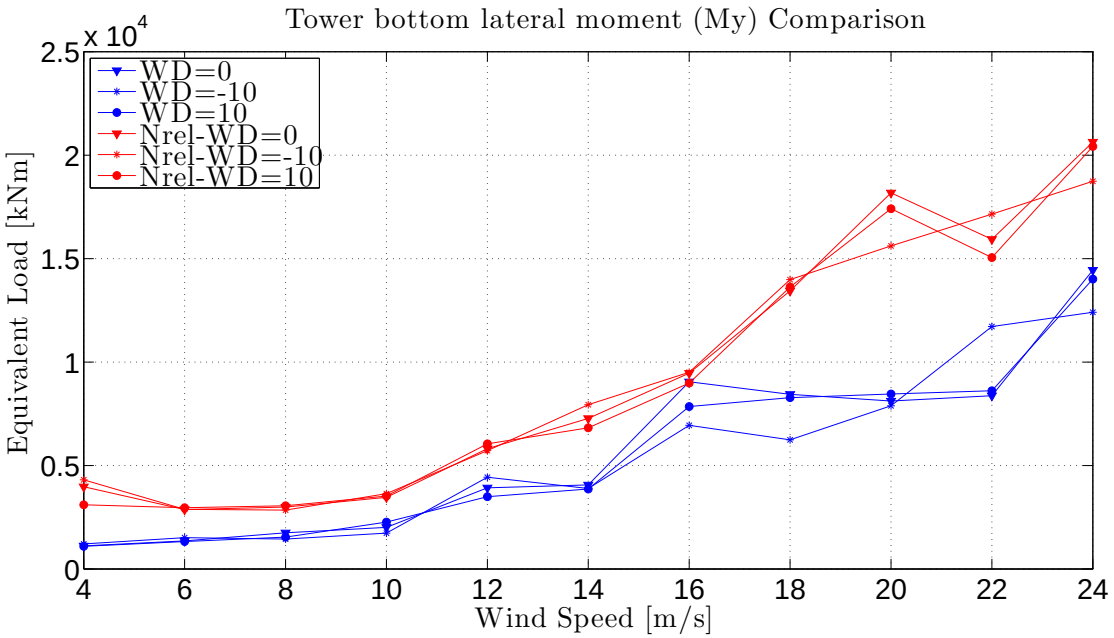

Figure 5.2: Tower bottom lateral moment (My) Comparison

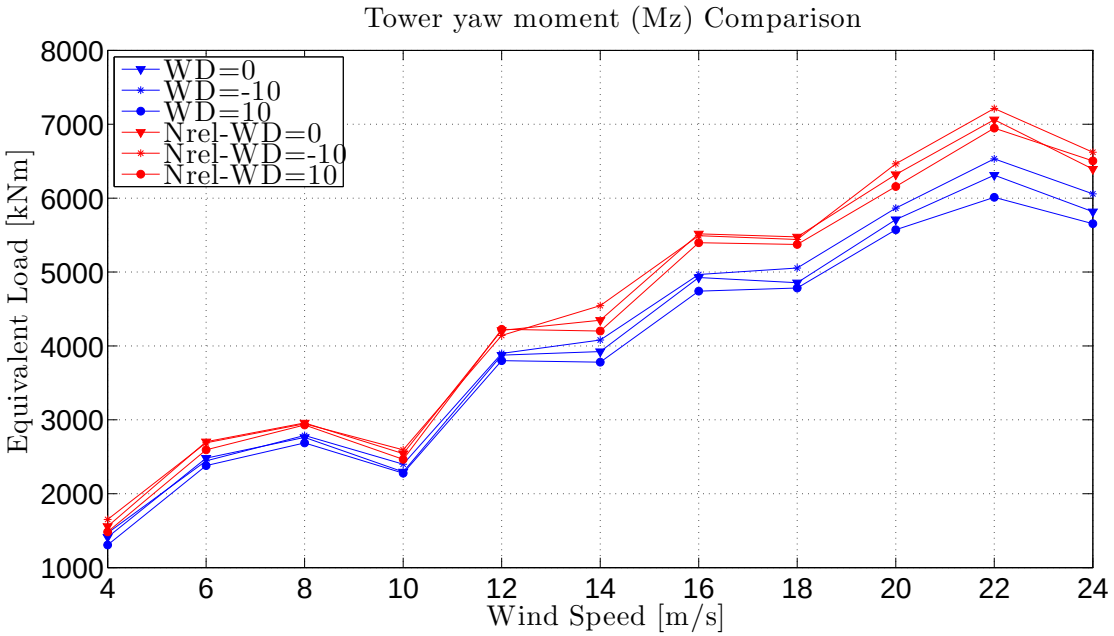

Figure 5.3: Tower yaw moment (Mz) Comparison

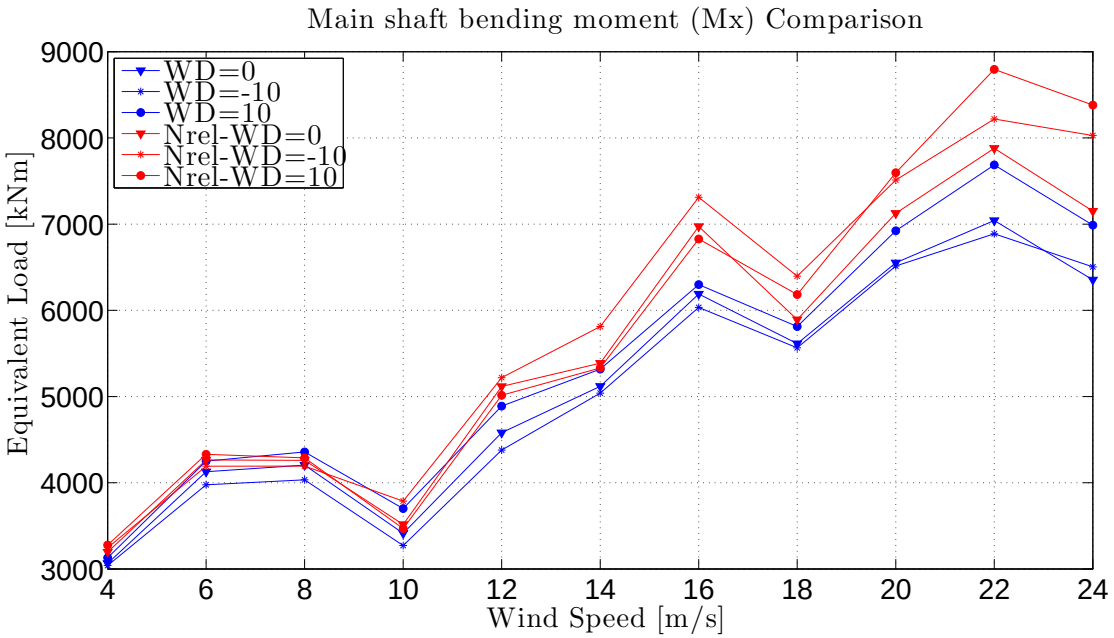

Figure 5.4: Main shaft bending moment (Mx) Comparison

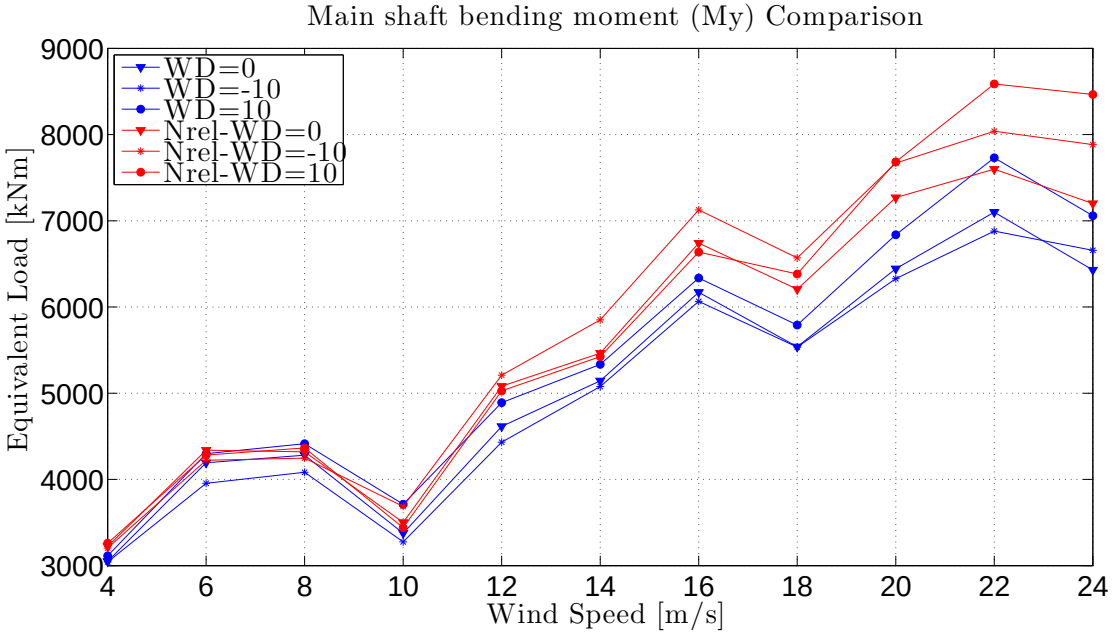

Figure 5.5: Main shaft bending moment (My) Comparison

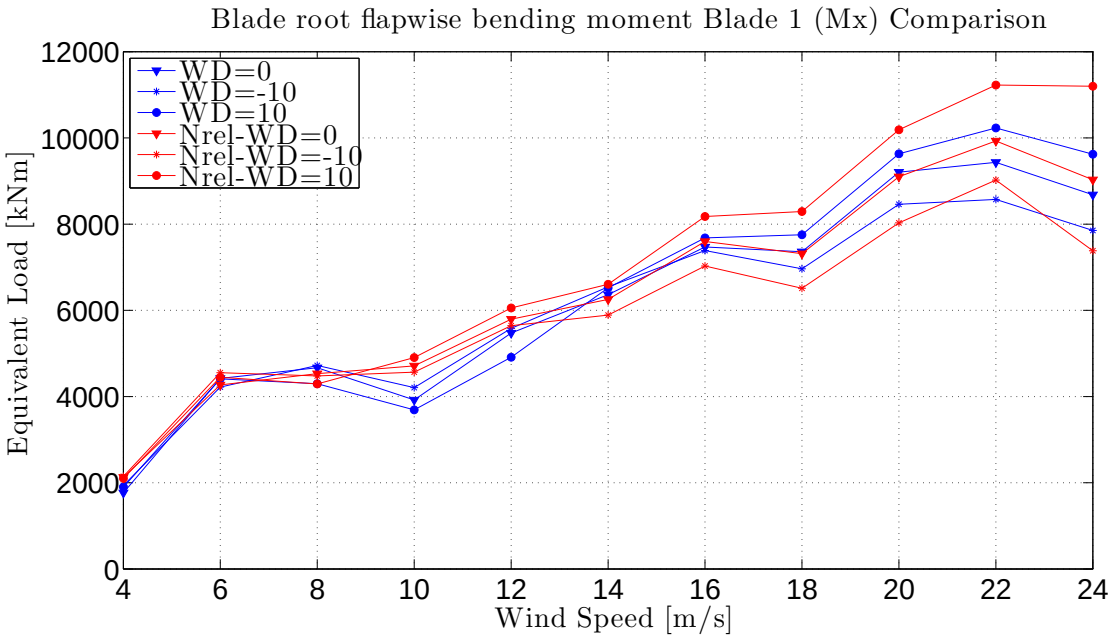

Figure 5.6: Blade root flapwise bending moment Blade 1 (Mx) Comparison

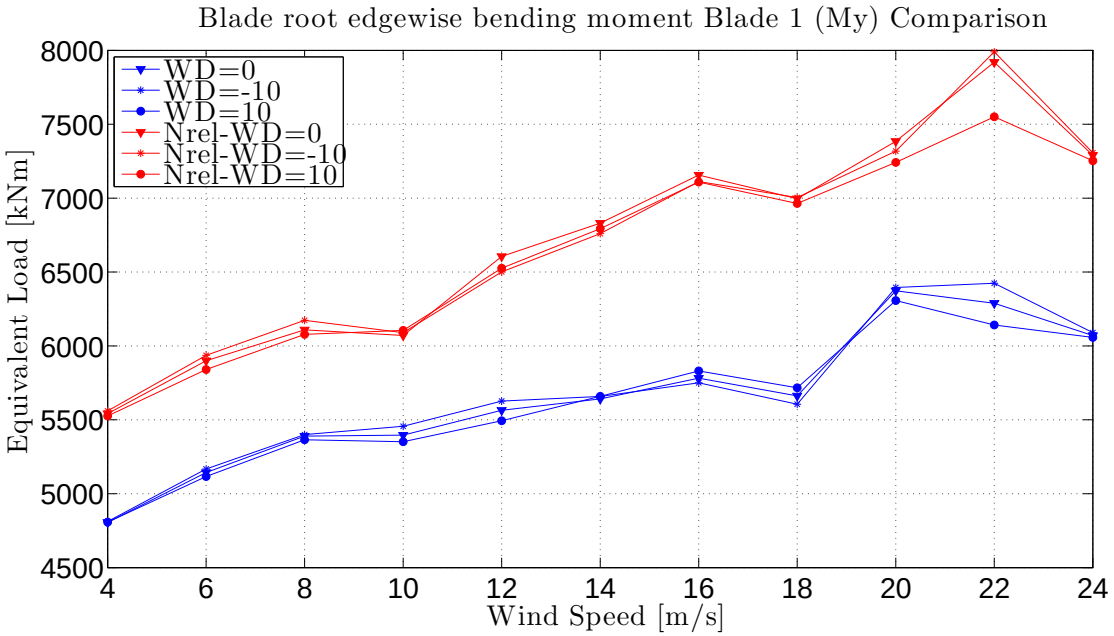

Figure 5.7: Blade root edgewise bending moment Blade 1 (My) Comparison

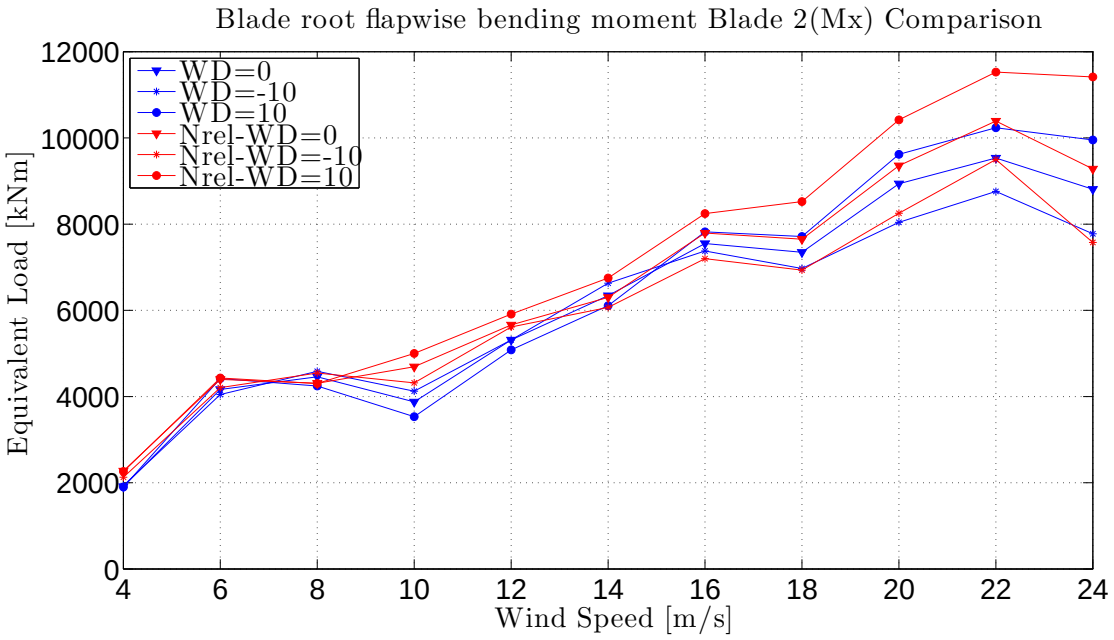

Figure 5.8: Blade root flapwise bending moment Blade 2 (Mx) Comparison

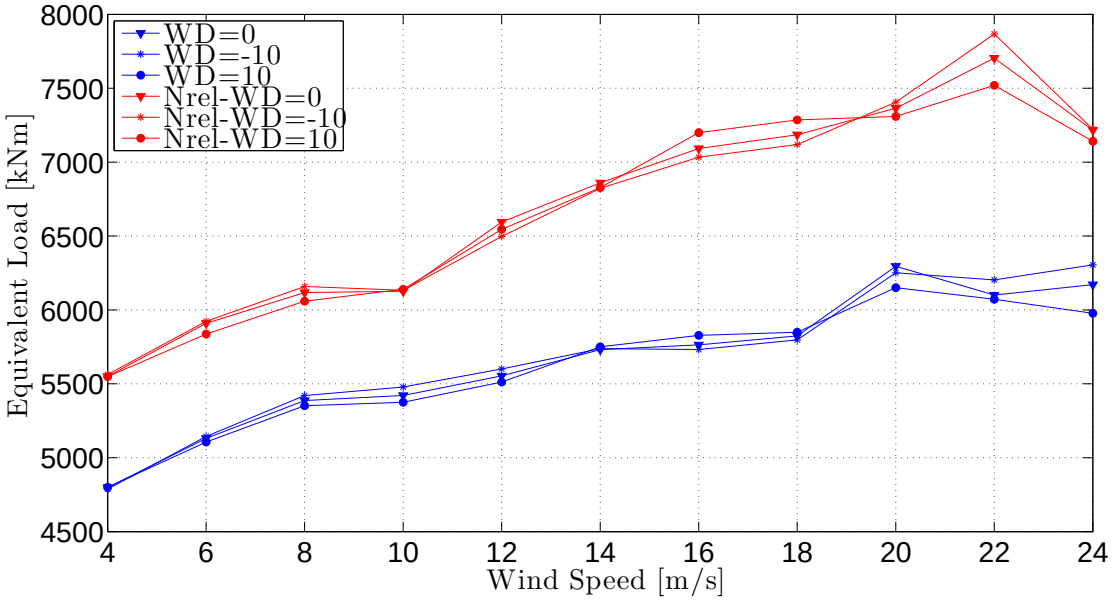

Figure 5.9: Blade root edgewise bending moment Blade 2 (My) Comparison

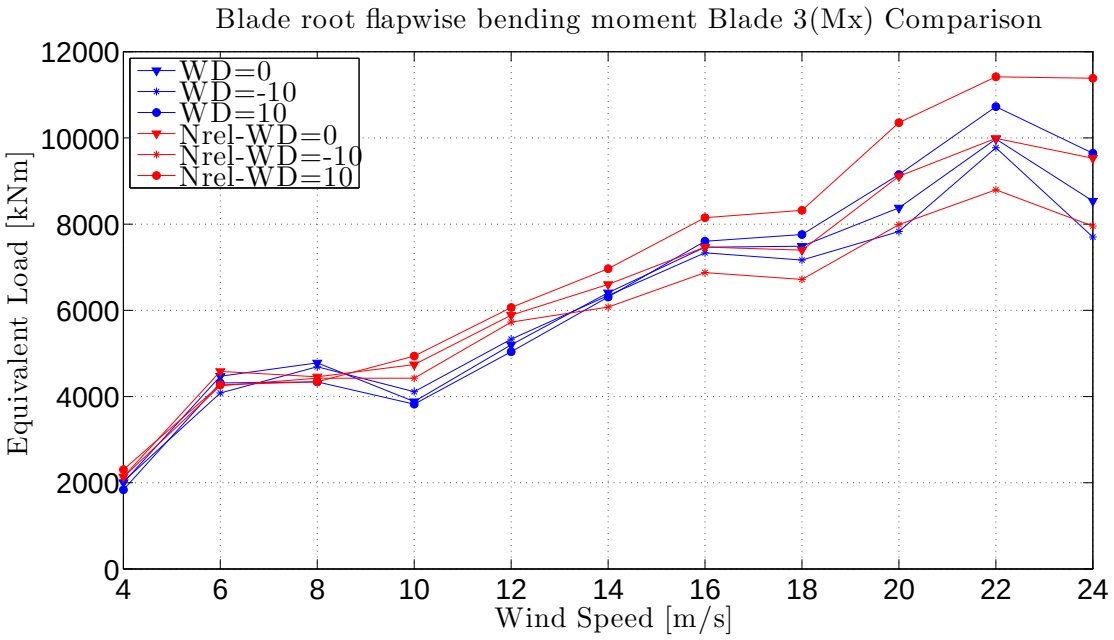

Figure 5.10: Blade root flapwise bending moment Blade 3(Mx) Comparison

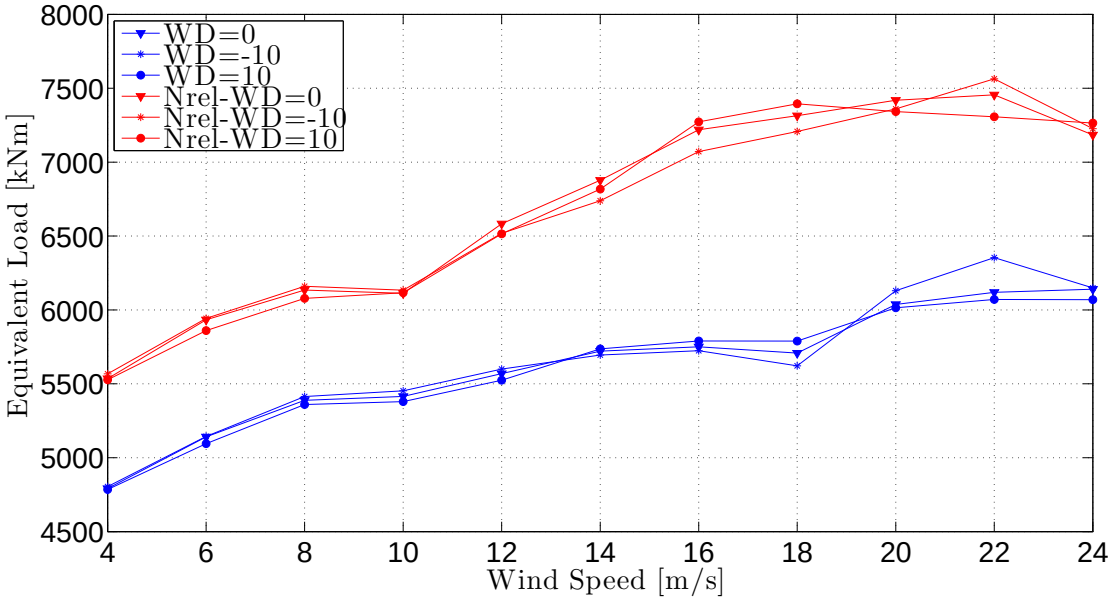

Figure 5.11: Blade root flapwise bending moment Blade 3 (My) Comparison

5.2 Statistical extrapolation of loads for ultimate load analysis

Following the IEC61400-1 standard, Annex F, an analysis of DLC 1.1 maxima for all wind speeds is carried out for the following bending moments (load processes):

- **Tower bottom longitudinal bending moment M_x.**
- **Tower bottom lateral bending moment M_y.**
- **Tower yaw moment M_z.**
- **Main shaft moment, M_x and M_y.**
- **Blade root flapwise bending moment, M_x, for all blades.**
- **Blade root edgewise bending moment, M_y, for all blades.**
- **Flapwise blade tip deflection, for all blades.**

This means that for each wind speed going from 4 m/s to 24 m/s, for each of the above mentioned channels, the following was done:

- For each load process, separately for yaw deviations of $-10°$, $0°$ and $10°$, respective threshold values were defined as the mean plus 1.4 times the standard deviation.
- The largest value between successive up-crossings of the respective thresholds were selected and collected as maxima for the corresponding load process, for all yaw cases, for the corresponding wind speed.
- The all-yaw maxima were normalised according to the largest load for that case and then Gumbel-fitted in order to calculate the corresponding α and β parameters.
- Equation 5.1 was used to sum over all wind speeds and thus obtain the exceedance probability for largest bending loads for all 7 channels, as depicted in 5.12.

$$P(M_{10min} > x) = 1 - F(x) \sim \sum_{i=1}^{N_v} (1 - F(x|V_i)^{n_i}) p(V_i) \tag{5.1}$$

The probability of each mean wind speed bin at hub height is given by the Rayleigh distribution, equation 5.2, (IEC61400-1, p.24) where $V_{average} = 0.2V_{ref}$ and $V_{ref} = 42.5$ m/s for Turkispain.

$$P(V_{hub}) = 1 - exp[-\pi(V_{hub}/2V_{average})^2] \tag{5.2}$$

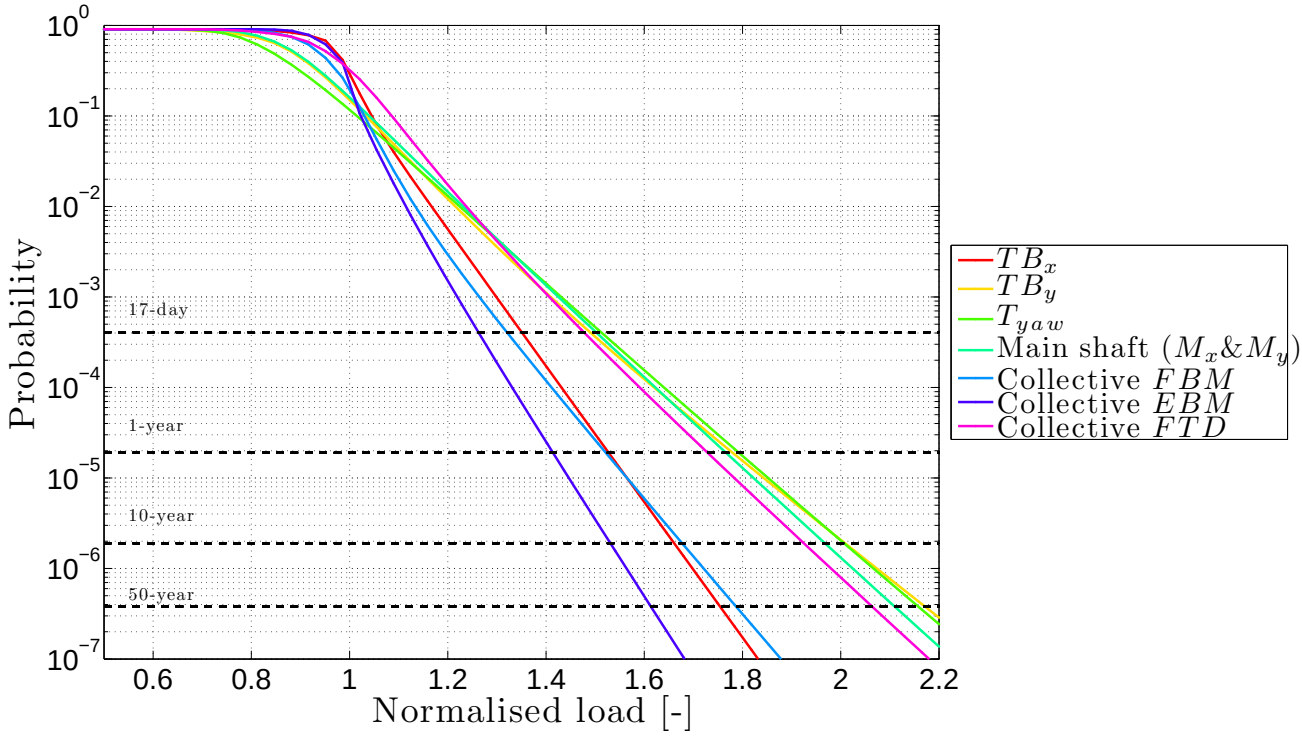

Figure 5.12: Exceedance probability for largest bending loads.

5.3 50-year NTM extremes vs ETM maxima

It is important to compare the 50-year extremes, estimated via the Gumbel Fitting method for normal turbulence load cases (NTM), with the maxima obtained from the extreme turbulent load cases (ETM), for each load process. The Gumbel 50-year extreme event prediction and maxima of extreme turbulence load cases are shown in tables 5.1 and 5.2, respectively. The channel names are stated in table 5.3.

Channel No. / Wind Speed [m/s]	2/[kNm]	3/[kNm]	7/[kNm]	11/[kNm]	14/[kNm]	15/[kNm]	24/[m]
4.00	28919.40	3297.62	3790.57	3997.29	4072.38	3207.03	4.06
6.00	65361.23	4533.88	7185.99	7648.68	11070.07	3515.39	4.04
8.00	64990.80	7592.38	8501.22	6595.12	11430.69	4035.29	5.84
10.00	68260.26	8748.01	6112.60	5020.10	11764.59	4600.78	6.05
12.00	85796.62	14191.25	11167.47	8711.16	13174.73	5058.32	7.27
14.00	92855.52	14424.44	11091.17	7823.56	12537.00	4618.85	6.12
16.00	72861.09	25276.59	14593.71	9232.63	10755.40	4472.71	7.33
18.00	79098.41	31107.46	13958.89	8322.15	11398.59	4168.44	8.45
20.00	76018.62	29500.95	15368.91	12267.16	11282.92	4267.54	10.65
22.00	80962.58	32892.60	22134.42	13238.30	13610.76	4642.96	10.00
24.00	81731.08	39825.21	18277.19	12268.58	9762.49	4893.12	10.67
26.00	74037.88	56135.13	18668.91	13220.56	10956.14	5518.43	11.36

Table 5.1: 50-year Gumbel fit.

Channel No. / Wind Speed [m/s]	2/[kNm]	3/[kNm]	7/[kNm]	11/[kNm]	14/[kNm]	15/[kNm]	24/[m]
4.00	21691.89	4658.66	3510.95	5391.58	4505.68	3497.31	5.20
6.00	55517.36	4872.87	6032.89	8492.22	12071.10	4475.65	5.89
8.00	62551.14	8676.07	8255.28	8520.13	12966.53	4867.52	6.67
10.00	65902.62	8037.93	5463.94	5935.84	12362.05	4772.67	6.21
12.00	74011.54	14243.26	8694.91	10032.10	13288.00	4773.93	6.82
14.00	70791.88	18075.07	8637.82	7968.80	12855.61	4605.67	6.54
16.00	75740.16	19746.69	10043.24	10707.33	14162.04	5090.44	7.85
18.00	65766.25	22896.01	10092.88	8871.65	11309.57	4470.63	8.19
20.00	63299.36	23912.09	9418.39	11874.55	12202.50	5592.67	10.30
22.00	59059.97	29797.18	12100.17	11367.15	11499.39	5159.76	9.46
24.00	54489.49	21360.61	10317.80	8926.02	11799.07	5161.83	9.48
26.00	62642.44	31152.64	9292.63	10915.11	11188.12	5798.02	11.16

Table 5.2: ETM maxima.

Channel No.	Load Type
2	Tower bottom longitudinal bending moment, M_x
3	Tower bottom lateral bending moment, M_y
7	Tower top yaw moment, M_z
11	Main shaft moment, M_x and M_y
14	Blade root flapwise bending moment, M_x, for all blades
15	Blade root edgewise belding moment, M_y, for all blades
24	Flapwise blade tip deflection

From the tables above, it can be concluded that, for some channels, Gumbel-predicted 50-year extremes exceeded ETM maximum values. Further simulations are required, increasing the turbulence levels in ETM until no load process or channel is exceeded by its NTM, Gumbel-predicted counterpart.

Chapter 6

Power Production

6.1 Power Curve

The power curve is calculated with HAWC2 simulations. The signal *generator electrical output* from the controller *.dll* was used, and 10-min average power production values for each wind speed were calculated. The power curve of Turkispain can be seen from figure 6.1.

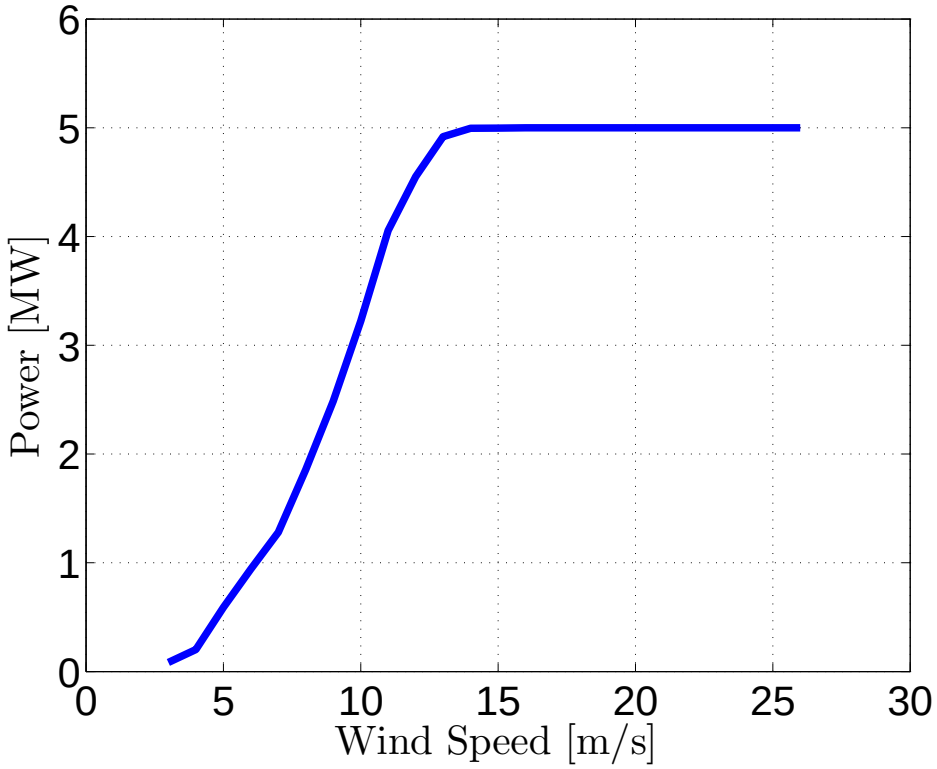

Figure 6.1: Turkispain's power curve.

6.2 Annual Energy Production

The annual energy production was calculated with respect to a Rayleigh distribution, as shown in figure 6.2. The selected wind climate is class II-B, i.e. $V_{ref} = 42.5m/s$ and turbulence intensity $I_{ref} = 0.14$ [IEC 61400-1 ©IEC 2005, p.22].

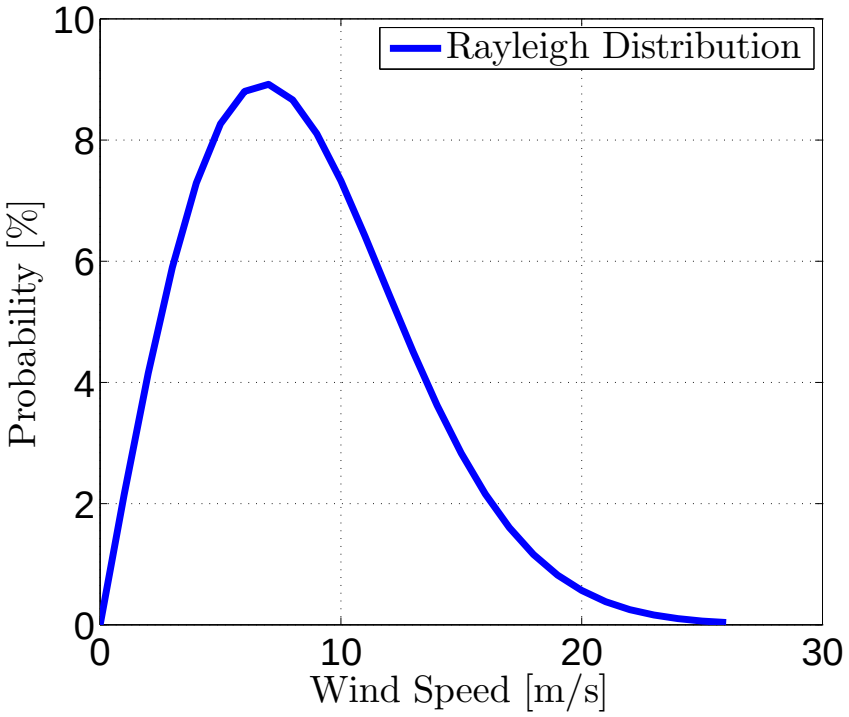

Figure 6.2: Interpolated sections.

According to the IEC61400-12-1 standard, p. 21, "a generic AEP is estimated by applying the measured power curve to different reference wind speed distributions." In order to do this, the mentioned Rayleigh distribution was used as the reference wind speed distribution. Equation 6.1 was used, for a certain number of bins, N.

$$AEP = N_h \sum_{i=1}^{N} [F(V_i) - F(V_{i-1})](\frac{P_{i-1} + P_i}{2}) \tag{6.1}$$

The estimations can be seen in table 6.1 and the AEP, with a highlight for $8.5m/s$, which is $V_{average} = 0.2V_{ref}$.

Wind Speed [m/s]	AEP [GWh]
4.00	4.03
4.50	5.54
5.00	7.22
5.50	9.04
6.00	10.93
6.50	12.85
7.00	14.74
7.50	16.58
8.00	18.33
8.50	**19.98**
9.00	21.51
9.50	22.91
10.00	24.18
10.50	25.32
11.00	26.30
11.50	27.15
12.00	27.86
12.50	28.43

Table 6.1: Rayleigh AEP estimation.

Chapter 7

Conclusion

This report is an attempt to complete a simplified aeroservoelastic design of a 5 MW wind turbine. In such processes, many iterations are required, since many parameters depend on each other. However, due to time limitations, this work is simplified precisely because it is a one-shot design project. The authors are aware of the fact that one-shot design is unlikely in real life design cases.

As a general conclusion, it can be said that the main goal stated in the introduction, which was to improve existing same class turbines (e.g. NREL and AREVA) was reasonably achieved. Evidently, a more in depth investigation is needed to draw a better conclusion. However:

- The blades are found to be lighter than NREL's.
- The tower, after the second iteration, is much lighter than NREL's. So generally less material is used.
- The fatigue analysis shows better results when both Turkispain and NREL were subject to the same wind climate. This means that Turkispain's lifetime can be expected to be longer, thereby the overall cost of energy is lower.